REDUCED ORDER AERODYNAMIC MODEL DEVELOPMENT OF ROAD/RACE VEHICLES

by

Jaclynn Mohrfeld Halterman

A dissertation submitted to the faculty of
The University of North Carolina at Charlotte
in partial fulfillment of the requirements
for the degree of Doctor of Philosophy in
Mechanical Engineering

Charlotte

2019

Approved by:

_____
Dr. Mesbah Uddin

_____
Dr. Peter Tkacik

_____
Dr. Matt Davies

_____
Dr. Srinivas Pulugurtha

_____
Dr. Heather Lipford

ABSTRACT

JACLYNN MOHRFELD HALTERMAN. Reduced order aerodynamic model development of road/race vehicles. (Under the direction of DR. MESBAH UDDIN)

This research systematically develops a real-time capable reduced order aerodynamic model of a race vehicle to predict the aerodynamic characterization of a transient vehicle. The aerodynamic model modularly combines the quasi steady state aerodynamic model and a transient aerodynamic model allowing independent development of each model. A new dual range quasi steady state model utilizing the independent variables of front ground clearance, rear ride height, and yaw is developed from wind tunnel data and demonstrates improved modeling capability relative to conventional aerodynamic models. While the quasi steady state aerodynamic model accurately predicts the aerodynamic coefficients of a static vehicle, the static vehicle aerodynamic coefficients are shown to significantly vary from the transient aerodynamic coefficients especially for drag, lift, and pitch moment. Thus, a transient aerodynamic model is necessary for accurate predictions. A transient aerodynamic reduced order model (ROM) utilizing the independent variable of pitch angle is developed from CFD results using a new model structure derived from analyzing the frequency response of the aerodynamic coefficients. The validation of the new transient ROM structure shows that the model better predicts the transient vehicle aerodynamic characteristics compared to the conventional transient ROM structure currently found in literature.

DEDICATION

This work is dedicated first to my parents, Jim and Helen Mohrfeld, for setting such a high bar and mentoring me throughout all the epic journeys in my life.

Secondly, to my loving husband, Tim Halterman, for being my rock throughout the whole PhD endeavor. We had no idea what to expect when I decided to go back to school to pursue my PhD, but he provided selfless support through the entire process. This dissertation and the research presented herein would not have been completed without him.

And finally, to my partners at Birdsong Brewing, especially Chandra Torence and Tina Crapsi, who provided the perfect words of encouragement to keep me focused on the finish line.

ACKNOWLEDGEMENTS

I would like to thank my adviser, Dr. Mesbah Uddin, for providing guidance and support throughout the PhD process. The direction provided for this research was invaluable and lead us to new and interesting findings.

I would also like to thank Chevy Performance for providing the data and vehicle geometry used in this research project and allowing us to publish the findings. The first and third papers would not have been possible without this information.

Finally, I would like to thank Charles Bounds for helping configure and prepare the vehicle geometry used in the final paper, and Adit Misar for helping with the physics configuration of the vehicle model enabling the transient simulation to converge.

TABLE OF CONTENTS

LIST OF FIGURES

LIST OF SYMBOLS

α Airfoil angle of attack (Paper 2); Vehicle pitch angle (Paper 3).

α_0 Pitch angle of transient model linerarization (Paper 3).

β Yaw angle of the vehicle (Paper 1).

γ^2_{xy} Coherence function (Paper 2).

A Amplitude of oscillation (Paper 2).

A Parametric fit coefficient for the unweighted model, f_1 (Paper 1).

B Parametric fit coefficient for the weighted model, f_2 (Paper 1).

c Chord (Paper 2).

C'_a Predicted aerodynamic coefficient (Paper 1).

C_1 ROM coefficient for α (Paper 2, Paper 3).

C_2 ROM coefficient for $\dot{\alpha}$ (Paper 2, Paper 3).

C_3 ROM coefficient for $\ddot{\alpha}$ (Paper 2, Paper 3).

C_4 Additional ROM coefficient for proposed transient ROM (Paper 3).

C_a Measured aerodynamic coefficient (Paper 1).

C_d Drag coefficient (Paper 2, Paper 3).

C_l Lift coefficient (Paper 2, Paper 3).

C_m Pitch moment coefficient (Paper 2).

C_{mx} Roll moment coefficient (Paper 3).

C_{my} Pitch moment coefficient (Paper 3).

C_{mz} Yaw moment coefficient (Paper 3).

C_{pitch} Pitch moment coefficient (Paper 1).

C_{pred} Predicted aerodynamic coefficient from complete aerodynamic model (Paper 3).

C_{QSS} Aerodynamic coefficient calculated from quasi steady state aerodynamic model (Paper 3).

C_s Side force coefficient (Paper 3).

C_T Aerodynamic coefficient calculated from transient aerodynamic model (Paper 3).

C_x Aerodynamic coefficient from CFD results (Paper 3).

f Frequency (Paper 2).

f_1 Unweighted mathematical model (Paper 1).

f_2 Weighted mathematical model (Paper 1).

H_d Frequency response of the drag coefficient to α (Paper 2, Paper 3).

H_l Frequency response of the lift coefficient to α (Paper 2, Paper 3).

H_m Frequency response of the pitch moment coefficient to α (Paper 2).

H_x Transfer function representing the transient aerodynamic model (Paper 3).

H_{d2} Frequency response of the drag coefficient to α^2 (Paper 2).

H_{my} Frequency response of the pitch moment coefficient to α (Paper 3).

K Quasi steady state aerodynamic model coefficients (Paper 3).

P'_m Deviation from the original coefficient P_{m0} (Paper 1).

P_n All parametric fit coefficients, A_n and B_n (Paper 1).

P_{m0} Original coefficient for each term in the aerodynamic model (Paper 1).

S'_m Sum squared error of perturbed coefficients (Paper 1).

S_0 Sum squared error of original coefficients (Paper 1).

S_n Sum squared error (Paper 1).

S_{xx} Auto spectral density of the system input (Paper 2).

S_{xy} Cross spectral density (Paper 2).

S_{yy} Auto spectral density of the system output (Paper 2).

T Length of signal used for auto or cross spectra density transformations (Paper 2).

W Weighting function (Paper 1).

w_1 Width of the transition section of the weighting function (Paper 1).

x Generic description of system input (Paper 2); Aerodynamic coefficient (Paper 3)

y Generic description of system output (Paper 2).

z_f Front ground clearance of the vehicle (Paper 1).

z_r Rear travel of the vehicle (Paper 1).

z_{fC} Cut-off value of the front ground clearance in the weighting function (Paper 1).

CHAPTER 1: INTRODUCTION

Vehicle dynamics models are used throughout the automotive and motorsports industries to predict the handling and performance characteristics of a vehicle in various maneuvers and drive cycles. Additionally, these models are used in real-time simulations such as driver-in-the-loop (DiL) and hardware-in-the-loop (HiL) simulators which require the vehicle model physics to compute in real-time, often in less than one millisecond. These use cases drive the need for accurate models with extremely quick run times. Simplified chassis and suspension models are typically used with parametric tire, engine, and quasi steady state aerodynamics models to achieve this performance [1]. Prior to this research, the aerodynamic modeling conducted in industry was unable to accurately model the aerodynamic characteristics of the vehicle as the nose of the vehicle moved in close proximity to the ground plane - a setup trend emerging in the motorsports industry to improve the race vehicle performance [3]. The transient vehicle aerodynamic behavior was also not captured in these industry standard models. Thus, the goal of this research is to develop a procedure to create an aerodynamic model accurately capturing the quasi steady state and transient aerodynamic characteristics of a race vehicle in its typical operating conditions.

The vehicle type used in this research is a Chevy NASCAR truck. The NASCAR truck is a race modified pickup truck which competes in a race series sanctioned by the National Association of Stock Car Auto Racing, NASCAR. This racing series competes at primarily oval style race tracks of various distances, bank angles, and vehicle top speeds, and the trucks can race at speeds up to 90 m/s at the faster tracks. At 90 m/s, the race vehicle can produce up to approximately 9 kN of downforce and 6 kN of drag. Compared to the approximately 16 kN weight of the vehicle, the

aerodynamic forces are a significant source of the loads on the vehicle, and thus are critical to be modeled accurately.

As the vehicle traverses the race track, the orientation of the vehicle with respect to the ground changes due to normal track curvature, banking, surface roughness, and the cornering of the vehicle. This results in the vehicle pitching, heaving, and yawing. The change in the vehicle orientation relative to the track significantly affects the aerodynamic forces and moments acting on the vehicle and these effects can be captured using a quasi steady state model. The change in the relative orientation with respect to time also affects the aerodynamic forces and moments requiring the need for a transient aerodynamic model as well.

The quasi steady state aerodynamic model is developed using wind tunnel data from a 2007 NASCAR truck. In 2007, the NASCAR truck reconfigured the lower front fascia to include a splitter, a configuration that is still raced today. The transient aerodynamic model is developed using computational fluid dynamics (CFD) with 2006 NASCAR truck geometry which includes a body style that differed slightly from the 2007 style and does not include a splitter. The change in model year is necessary for for two reasons. First, geometry for the 2007 NASCAR truck was unavailable to the researcher. And second, since the body of style of the 2007 truck is still raced today, the results obtained from this research would not have been approved by Chevy Performance for journal publication for intellectual property reasons. Due to the difference in body styles, much of the development of the quasi-steady state and transient aerodynamic models is focused around the procedure for the aerodynamic model develop such that the procedure can be applied to any vehicle in the future.

The aerodynamic model proposed throughout this research is structured such that the quasi steady state and transient aerodynamic models can be develop modularly. This is achieved using the proposed aerodynamic model structure in figure 1.1 where $C_{pred,x}$ is the aerodynamic coefficient for each of the x coefficients - drag, side force,

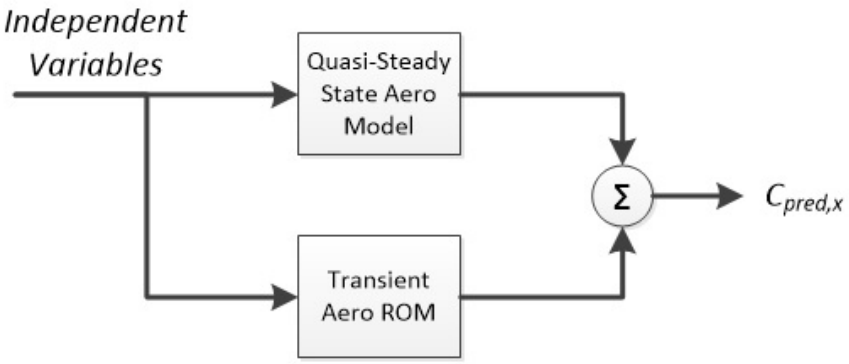

Figure 1.1: Proposed aerodynamic model structure

lift, roll moment, pitch moment, and yaw moment.

The quasi steady state aerodynamic model development is documented in the first paper included in Chapter 2. The aerodynamic coefficients are shown to be highly nonlinear with respect to the independent variables - front ground clearance, rear ride height, and yaw - especially as the nose of the vehicle moves closer to the ground. A smoothly transitioning dual range model is developed to fit the pitch moment aerodynamic coefficient accurately when the vehicle operates both close to the ground and in the non ground effected operating ranges. A model complexity reduction process is then applied to the aerodynamic model to reduce the data requirements for developing the aerodynamic model. The pitch moment coefficient is the only aerodynamic coefficient model developed in this paper, but the same systematic quasi steady state aerodynamic model development can be extended to the other five aerodynamic degrees of freedom to develop a complete six degree of freedom quasi steady state aerodynamic model for any vehicle. [3]

Furthering the research presented in the first paper, the fit error of the dual range quasi steady state aerodynamic model is compared to the fit error from a conventional aerodynamic model, and the new dual range aerodynamic model is shown to better fit the wind tunnel data. To determine if the improvement in the quasi steady state aerodynamic model affects the prediction of vehicle performance an additional research

project is conducted. Both the dual range quasi steady state aerodynamic model and the conventional aerodynamic model are independently applied to a multi-body vehicle model in quasi steady state simulations to analyze the effects of the aerodynamic model on handling, maximum corner speed, and drive force metrics. The increased accuracy of the high fidelity aerodynamic model is found to have realizable effects on the performance metric predictions. [2] This research paper is not included in this dissertation due to the university's dissertation copyright regulations.

With an improved quasi steady state aerodynamic model, the research focus shifts to develop a transient aerodynamic model. The transient aerodynamic model is developed using CFD results instead of wind tunnel results as transient wind tunnel testing in commercially available North American wind tunnels are unable to capture accurate transient responses due to the vehicle restraint systems, the low bandwidth of the vehicle orientation actuation system, and the experimental noise of the wind tunnels.

The transient aerodynamic model is developed as a reduced order model (ROM) to meet the run time requirements for the DiL and HiL operations. The transient CFD simulation requires over 500x real time to process the simulation results using 128 cores, and most DiL and HiL test rigs are not equip even with this level of processing power.

Prior to utilizing CFD to develop a transient ROM on a complex vehicle model, a process for the transient ROM development is created using a simple 2-D NACA0012 airfoil with a direct numerical simulation (DNS) CFD numerical method. This transient ROM development process is captured in the second paper in this dissertation included in Chapter 3. A systematic process is employed to develop the ROMs for each aerodynamic coefficient - drag, lift, and pitch moment. First, a CFD simulation is conducted to determine the linearity of each system. If a nonlinear relationship between the input and output is identified, the system is restructured as a nonlinear

operator followed by a linear system to allow for the use of linear system identification techniques. A second CFD simulation is conducted to determine the frequency response of each linear system, and the coefficients of each ROM are extracted by fitting a second order model to each frequency response function. The ROMs are validated against an independent CFD simulation of a pitching airfoil and are shown to accurately model each aerodynamic coefficient.

The linear system identification techniques successfully employed in developing the transient ROMs for the airfoil are applied in the development of the transient ROMs for the vehicle model. While the quasi steady state models utilized three independent variables, the transient model development only begins with analyzing a single independent variable, pitch angle. There is intent to continue this research to develop ROMs for additional independent variables utilizing the same model development procedure described in this research.

The development of the transient aerodynamic vehicle ROM is the final paper included in this dissertation in Chapter 4. Unsteady Reynolds-averaged Navier-Stokes (URANS) CFD simulations are conducted on both a static vehicle and a transient vehicle undergoing pitching motion. The aerodynamic results are shown to significantly differ between the static and transient simulations for the aerodynamic coefficients of drag, lift, and pitch moment. For the other three coefficients, side force, roll moment, and yaw moment, the steady state results were shown to capture the transient results well, so no additional transient aerodynamic models are developed for these three aerodynamic coefficients. The transient ROMs developed for the drag, lift, and pitch moment are developed in a similar fashion to those of the airfoil; however, the structure of the transient airfoil model, which is the same as the structure of transient vehicle aerodynamic models found in literature, did not achieve the desired level of accuracy in modeling the aerodynamic coefficients. The structure of the aerodynamic model was thus modified based on the frequency response shape of the CFD results.

The results of this modified transient aerodynamic ROM structure correlated well to the results of a separate transient CFD simulation, and the transient ROM results showed a significant improvement in predictive capability of the transient aerodynamics coefficients compared to the quasi steady state aerodynamic model alone.

The research presented in this dissertation focuses on the design and development of a new, higher fidelity aerodynamic vehicle model capable of predicting the aerodynamic force and moment coefficients of a transient vehicle as it traverses the race track. An improved quasi steady state aerodynamic model is developed and shown to capture the quasi steady state aerodynamic coefficient prediction better than conventional models. Transient vehicle aerodynamic ROMs are also developed and validated to predict the aerodynamic coefficients relative to the vehicle pitch angle, and the new proposed transient ROM structure is shown to better predict the transient aerodynamic characteristics than the conventional ROM structure published in literature. The results from the transient vehicle CFD simulations also reveal that the quasi steady state model alone is unable to accurately predict the aerodynamic coefficients of drag, lift, and pitch moment, and the inclusion of the transient ROM for these coefficients is required for an accurate vehicle aerodynamic model.

CHAPTER 2: (PAPER 1) QUASI STEADY STATE AERODYNAMIC MODEL DEVELOPMENT FOR RACE VEHICLE SIMULATIONS

2.1 Introduction

Developing race car vehicle dynamic simulations requires accurate modeling of every vehicle subsystem including the aerodynamic model - the mathematical model of the aerodynamic forces and moments acting on the vehicle as a function of the vehicle orientation which includes the front ground clearance, rear ride height and yaw. These aerodynamic forces and moments can vary based on the position of the vehicle relative to the ground plane and the wind direction (the effective yaw) [13, 11, 10, 2]. Additionally, the race vehicle is subjected to differing conditions on the race track such as wind gusts and vehicle proximity that result in turbulence intensity and length scale variations that further effect the aerodynamic forces and moments. To the best of the author's knowledge there is no literature on the effect of these dynamic variations on race vehicle aerodynamic characteristics. Prior to generating an aerodynamic model accounting for these unknown dynamic effects, an accurate quasi steady state aerodynamic model must first be developed. Future work can then be conducted to develop more advanced time-varying aerodynamic models in addition to the quasi steady state model.

The race vehicle aerodynamic model must provide solutions with a quick turnaround time to allow for implementation in a track side simulation analysis tool. Such simulation tools are a necessity in the motorsports industry to analyze and optimize vehicle setups based on race day track and weather conditions. Motorsports simulations exercise a vehicle model populated with track side tunable vehicle setup information, i.e. suspension geometry, stiffness elements such as springs, and damping elements such

as shocks, to determine the vehicle response to the track and driver inputs. Other components of the vehicle model include subsystems that are not tunable on a race to race basis such as engine models, tire models, and aerodynamic models. These subsystem models are equally as important to generating the proper vehicle response and therefore must be model accurately. Since the aerodynamic models do not vary on a race to race basis, a single aerodynamic model can be developed and applied to the vehicle simulations given the same race vehicle body style.

The aerodynamic model captures the effects of the vehicle orientation on the aerodynamic forces and moments acting on the vehicle. The forces and moments acting on the vehicle model can be measured from wind tunnel testing at various ride height and yaw configurations of the vehicle in the tunnel. The measured force and moment data can then be fit with a mathematical model to be utilized in the vehicle simulation. This empirical model allows for quick solution time and thus lends itself to motorsports vehicle simulation integration.

Another potential method to calculate the aerodynamic forces and moments is utilizing computational fluid dynamics (CFD). However, generating a CFD solution is slow and does not meet the runtime requirements of a trackside vehicle simulation tool. This fast turnaround time requirement eliminates the likelihood of a CFD based solution; therefore, industry practice has evolved to creating parametric aerodynamic predictive models based on wind tunnel data.

Quasi steady state aerodynamic models have been implemented in vehicle dynamic simulations with varying degrees of complexity. Original steady state models used constant aero fores or coefficients with no vehicle orientation dependencies [5, 6]. As wind tunnel testing of vehicles furthered, the effect of yaw on the aerodynamic forces and moments was documented [13, 11, 10] and incorporated into aerodynamic modeling of vehicle simulations [15, 9]. The next step in quasi steady state model development came with the inclusion of front and rear vehicle travels as dependencies

of the aerodynamic model [2]. More recently, the effect of individual race vehicle body components, such as wings, have begun to be characterized and modeled in vehicle dynamic simulations [3].

The original aerodynamic models only included three degrees of freedom: front lift, rear lift, and drag [5, 6, 15, 9, 2]. Additional degrees of freedom were then added to these models to include side force and yaw moment[4]. The final degree of freedom, the roll moment, was later added to vehicle models for complete modeling of all aerodynamic forces and moments acing on the vehicle [15].

The development of the mathematical equations used to model the quasi steady state aerodynamic model were first developed in the aerospace field [8]. Second order polynomial fits were applied to the aerodynamic model independent variables and used to calculate the aerodynamic forces acting on an aircraft. This concept was later extended to apply to automobiles by modeling the aero forces as second order polynomial fits of front and rear ride height [7]. There is little other documentation in literature on the evolution of this modeling technique; however, typical industry practice now develops full or partial second order surface fits over the range of independent variables tested. These independent variable are typically front travel, rear travel, and yaw angle as identified in the aforementioned literature.

In recent years, however, race vehicles have found performance improvements by traveling the vehicle closer to the ground. Wind tunnel testing has shown that vehicle downforce is increased and drag is decreased as the leading edge of the vehicle is closer to the ground. For instance, in all of the three official racing series, viz. Sprint Cup, XFINITY and Camping World Truck Series, managed by America's National Association for Stock Car Auto Racing, popularly knows as NASCAR, the current setup trends attempt to minimize the front ground clearance of the vehicles. In some cases, the leading edge of the vehicle intentionally makes contact with the track, usually over bumps, to maintain low front ground clearance throughout the remainder

of the track. In these conditions, as the authors' have observed, second order fits are no longer accurate enough to model the quasi steady state aerodynamic forces and moments. The aerodynamic forces and moments become highly nonlinear as the vehicle maintains an attitude with low front ground clearance. A new mathematical model is proposed in this paper to accurately model the current wind tunnel quasi steady state aerodynamic data.

The wind tunnel data presented in this paper was collected at the AeroDyn Wind Tunnel in Mooresville, North Carolina, USA using a 2007 NASCAR truck series vehicle. This testing measures the aerodynamic forces and moments at various vehicle orientations by varying three vehicle positions: front travel, rear travel, and yaw angle. The test plan was designed to gather adequate data to allow for each force and moment to be properly fit with the mathematical model. As the parameters in the mathematical model increase to more accurately fit the data, the amount of required wind tunnel data also increases.

Wind tunnel testing is time consuming and very expensive. Testing at AeroDyn, where the datasets for the current work were acquired, costs $1895/hour [1]. A test plan for steady state aerodynamic mapping can take up to five hours of tunnel-time; thus costing almost $10,000 at AeroDyn. Other commercially available test facilities may be even more costly; for example, Windshear, a full scale rolling-road wind tunnel in Concord, North Carolina, charges a new customer $35000 for a one-off 10-hour shift [16]. Reducing the size of the test plan can reduce both the cost and the time requirements of testing. Previous research efforts to reduce test runs utilized design of experiments (DOEs) [12, 14]; however, these results do not achieve the accuracy of the model required due to the coarser distributions of the independent variables.

Minimizing the complexity of the mathematical model while maintaining accurate modeling results will allow for the amount of test data to be reduced with no cost

to the aerodynamic model. A procedure for systematically reducing the number of terms in the mathematical model while maintaining an acceptable level in modeling error has been developed and presented in this paper. Applying this procedure to the new fit equation results in accurate quasi steady state aerodynamic models ideal for implementation into a race vehicle simulation.

2.2 Quasi Steady State Aerodynamic Model Development

The nonlinearity of the quasi steady state wind tunnel data appears primarily in the aerodynamic moment coefficients. Figure 2.1 contains the plots of the aerodynamic moment coefficients vs. the front ground clearance of the race vehicle, z_f, at a constant rear travel, z_r, and yaw angle, β. A model with more complexity than commonly used second order models is required to accurately fit this data. In observing the data, it is hypothesized that the lower ground clearance data and the higher ground clearance data could be better modeled if an additional mathematical model is applied to one section of the ground clearance data. Expanding upon this concept, an aerodynamic model with two mathematical model terms is developed. One mathematical model applies to the entire range of data, and the second mathematical model is weighted to only apply to the higher front ground clearance data.

On the basis of the discussion above, the authors' propose an aerodynamic model equation:

$$C'_a(z_f, z_r, \beta) = f_1(z_f, z_r, \beta) + W(z_f)\Big(f_2(z_f, z_r, \beta)\Big), \tag{2.1}$$

where C'_a is the predicted aerodynamic coefficient (force or moment), f_1 is the un-weighted mathematical model, f_2 is the weighted mathematical model, and W is the weighting function that is a function of the front ground clearance. Essentially, f_2 is a deviation function that contributes to the low-ground clearance discrepancies observed in the "currently industry wide popular" second order fit. The weighting

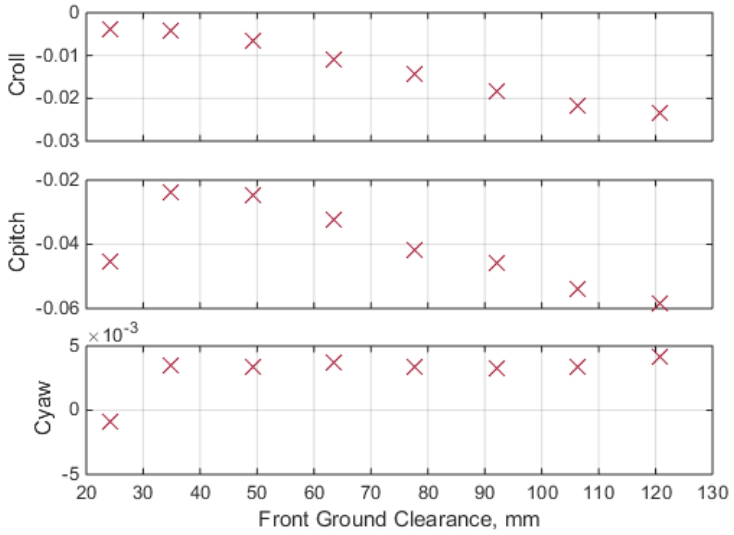

Figure 2.1: Aerodynamic moment coefficients vs. front ground clearance at a set rear ride height and yaw angle; Top: Roll moment; Middle: Pitch moment; Bottom: Yaw moment

function W is conjectured to have the form:

$$W(z_f) = \frac{1}{2} + \frac{1}{2}\tanh\left(w_1\left(z_f - z_{f_C}\right)\right) \tag{2.2}$$

and is illustrated in figure 2.2. This weighting function drives the weighting of f_2 to 0 at low front ground clearance values below a cut-off value of $z_f < z_{f_C}$, and maintains the weighting of f_2 at 1 for the higher ground clearance values. The other variable in the equation, w_1, influences the width of the transition section of the function.

Each mathematical model term, f_1 and f_2, in equation 2.1 are proposed to be functions of front ground clearance (z_f), rear ride height (z_r), and yaw (β). Since f_1 has no weighting, the model must remain valid over the entire range of data. Thus, based on the trends observed as in figure 2.1, only a linear dependency of the front ground clearance, z_f is included in the model function f_1. A second order dependency of f_1 on rear ride height and yaw seems consistent with the findings in literature

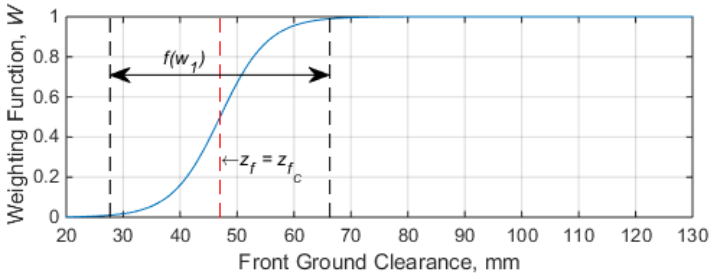

Figure 2.2: Weighting function

[13, 11, 10, 2, 15, 9] and current modeling practices prevalent in the industry. Thus, the function f_1 is defined as

$$f_1(z_f, z_r, \beta) = \sum_{i=0}^{1}\sum_{j=0}^{2}\sum_{k=0}^{2} A_{i,j,k}(z_f)^i(z_r)^j(\beta)^k, \tag{2.3}$$

where $A_{i,j,k}$ is the parametric fit coefficient for each term. Since there are two possible values for i and three possible values for j and k, there are $2 \times 3 \times 3$, or 18, terms in this equation. Thus, there will be 18 model coefficients in the f_1 fit. For the higher ground clearance f_2 fit, the surface is a second order function of each independent variable and can be defined as

$$f_2(z_f, z_r, \beta) = \sum_{i=0}^{2}\sum_{j=0}^{2}\sum_{k=0}^{2} B_{i,j,k}(z_f)^i(z_r)^j(\beta)^k, \tag{2.4}$$

where $B_{i,j,k}$ is the parametric fit coefficient for each term of the model. In this equation there are now three possible values i as well as j and k yielding $3 \times 3 \times 3$, or 27 terms and thus 27 total parameters in the f_2 fit.

Between equations 2.2, 2.3, and 2.4 there are 47 coefficients that must be determined to generate the aerodynamic model given in 2.1. An iterative least squares approach is used to calculate the fit coefficients. First, a reasonable starting range for w_1 and z_{f_C} is evaluated for the fitting process. For each of n combinations, $w_1^{(n)}$

and $z_{f_C}^{(n)}$, of w_1 and z_{f_C}, a linear least squares fit is applied to calculate the values of $A_{i,j,k}$ and $B_{i,j,k}$. This is represented in the equation below

$$P_n = \left(X_n^T X_n\right)^{-1} X_n^T C_a \tag{2.5}$$

where $P_n = [A_n, B_n]^T$, C_a is a $1 \times p$ matrix of one degree of freedom of the measured aerodynamic coefficients, and X_n is a $p \times m$ matrix of each model parameter from equation 2.1 evaluated using $w_1^{(n)}$ and $z_{f_C}^{(n)}$ where p is the sample size of the data and m is the number of parameters in the fit.

For each n, the sum square error is calculated as

$$S_n = \sum_{l=1}^{p} \left(C_{a,l} - f([z_{f,l}], [z_{r,l}], \beta_l, P_n)\right)^2 \tag{2.6}$$

and the final set of coefficients, P, equals the P_n which minimizes S_n.

The aerodynamic model described in equation 2.1 utilizes every term and cross term of the inputs. However, not all of these parameters may be necessary for a model with sufficient engineering accuracy. A reduction in the number of parameters would reduce the number of tunnel-test data points required to develop the model, thereby reducing test time and costs for quasi steady state aerodynamic wind tunnel testing. To determine the high impact parameters of the model, the effects of each parameter on the model accuracy is determined, and the parameters that are found to not have a significant impact on the goodness of the fit are removed from the mathematical models. This is achieved by numerically determining the partial derivative of the modeling error with respect to each parameter as

$$\frac{\partial S}{\partial P_m} = \frac{S'_m - S_0}{P'_m - P_{m0}} \tag{2.7}$$

where P_{m0} is the original coefficient of each parameter, P'_m is a small deviation from

the original coefficient value, and

$$S_0 = \sum_{l=1}^{p} \left(C_{a,l} - f([z_{f,l}], [z_{r,l}], \beta_l, P_{m0})\right)^2 \tag{2.8}$$

$$S'_m = \sum_{l=1}^{p} \left(C_{a,l} - f([z_{f,l}], [z_{r,l}], \beta_l, P'_m)\right)^2 \tag{2.9}$$

The parameters with partial derivatives that have the least effect on the model error, or the smallest $\partial S/\partial P_m$ values, are removed from the model, and new coefficients are calculated for the remaining parameters using the procedure outlined above. This process of elimination of the least significant modeling parameter(s) from the aerodynamic mathematical model continued until the error of the model exceeds a set threshold.

This quasi steady state aerodynamic model development approach is applied to pitch moment coefficient for the demonstrative purposes of this paper. This technique can be extended to each aerodynamic degree of freedom to accurately model each aerodynamic force and moment coefficient.

2.3 Initial QSS Aerodynamic Model Results

Applying the model in equation 2.1 to the pitch moment coefficient results in a accurate fit of the raw wind tunnel data. The resulting model errors are plotted in figure 2.3. The error is within 3 counts for all the data points, and 95% of the data fit within 2 counts[1]. The error in this fit is less than the uncertainty in the wind tunnel measurements. For a more intuitive understanding, each count of pitch moment is equivalent to about 22.5 Nm acting on the race vehicle at a common cornering speed of 170 mph, so the error of the initial fit is within 67.5 Nm of the measured pitch moment.

[1] A count is equivalent to a 0.001 change in the aerodynamic coefficient.

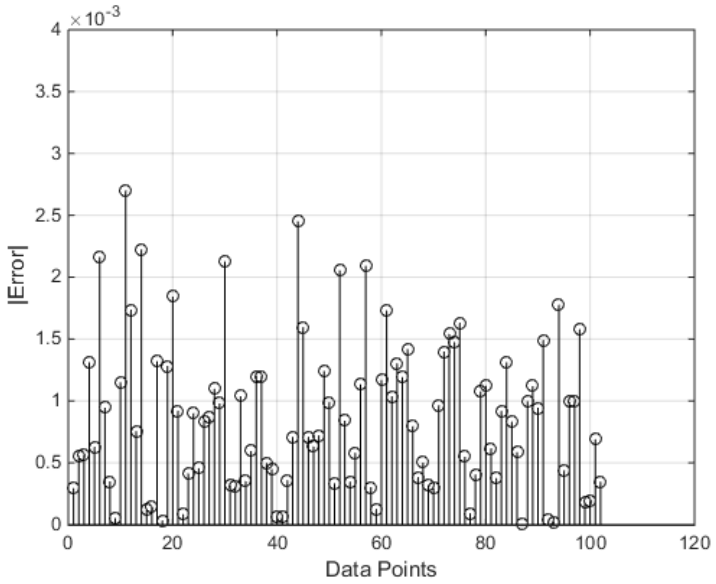

Figure 2.3: Error of original fit at each data point

2.4 QSS Aerodynamic Model Parameter Reduction

The parameter reduction procedure is applied to the initial pitch moment model to simplify the model by removing parameters that have minimal effect on the modeling accuracy. The partial derivative of the model error with respect to each model parameter is evaluated and plotted in figure 2.4. Many parameters are revealed to have minimal effects on the error and will thus have minimal impact on the accuracy of the mathematical model.

Beginning with the parameter with the least effect on the error and including parameters in order of increasing error significance, each parameter is removed from the model, and new model coefficients are generated. The error is calculated for each new model and plotted against the number of decreased parameters in figure 2.5.

As the model decreases in parameters, the error increases. Two larger steps in the error occur as parameters are removed from the initial model. One step occurs after nine parameters are removed, and the other step occurs after 17 parameters are removed. The error at each data point of these two reduced parameter models is

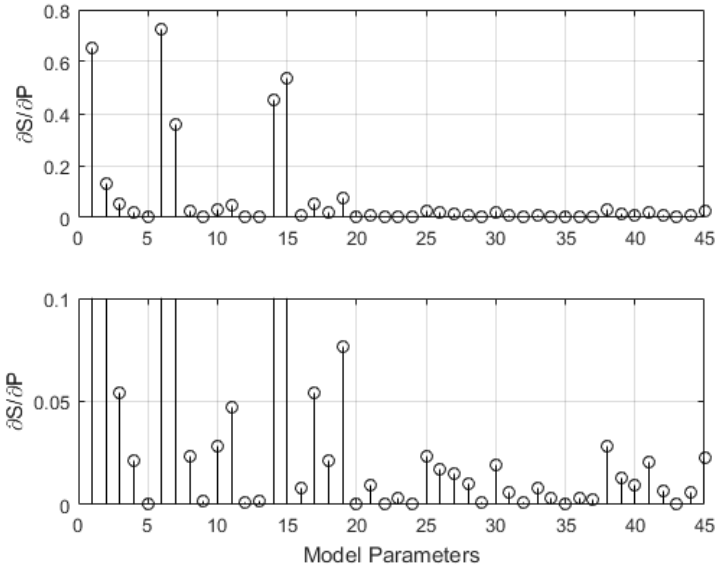

Figure 2.4: Partial derivative of the sum squared error with respect to each fit parameter; Top: All fit parameters; Bottom: Zoomed view of top plot to reveal the parameters with smaller error effects

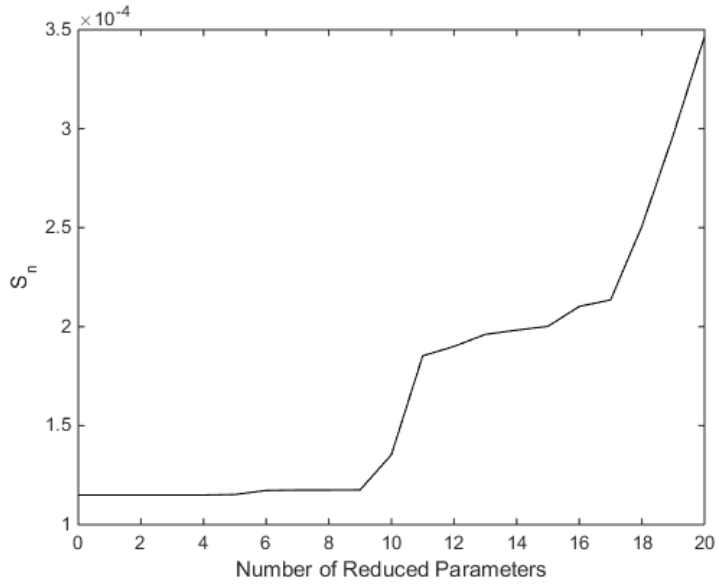

Figure 2.5: Fit error versus number of terms removed from fit

presented in figures 2.6 and 2.7.

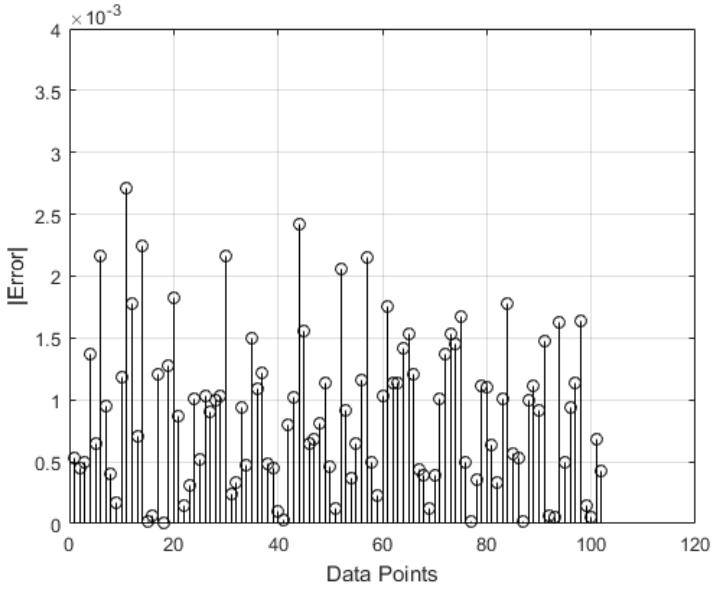

Figure 2.6: Error of reduced term fit, less 9 terms

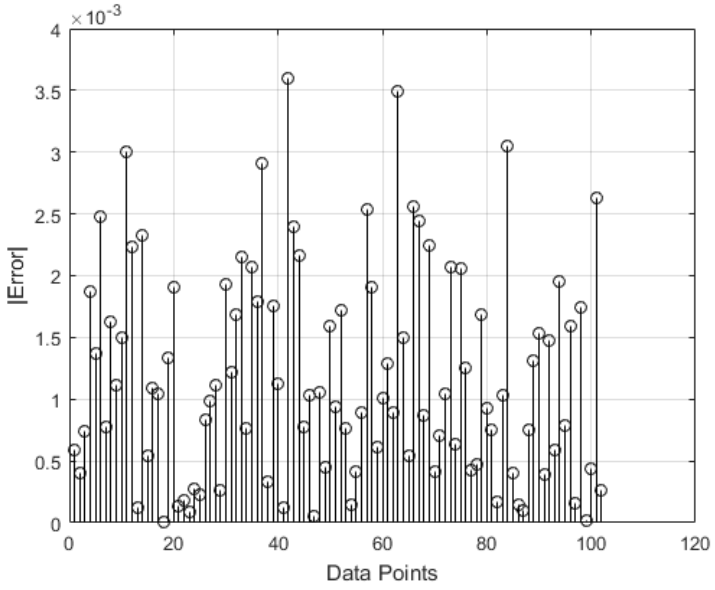

Figure 2.7: Error of reduced term fit, less 17 terms

The magnitude of the error is expectedly less from the model with only nine parameters removed; however, this model contains 38 parameters as opposed to the 30

parameters in the other model. Reducing the parameters will reduce the required wind tunnel data and thus testing time and cost, but there is a trade off in model accuracy. Since the fidelity of the model is important to accurate vehicle simulation results, the 38 parameter model is selected for the final quasi steady state aerodynamic model. If higher fidelity models are not as important as testing time and cost, then the further reduced parameter model could be used.

2.5 Reduced Parameter QSS Aerodynamic Model Results

The results of the final reduced parameter model are plotted with the original wind tunnel data points in figures 2.8, 2.9, and 2.10 for 0, -2, and -3 degrees of yaw respectively. In each figure, the fits are plotted against the front ground clearance for each rear ride height tested. The model results capture the nonlinear trend of the pitch moment coefficient as a function of front ground clearance.

The aerodynamic model can also be analyzed to ascertain the effects of rear ride height and yaw on the aerodynamic coefficients. Figure 2.11 contains plots of the pitch moment at two different yaw angles and multiple front ground clearances. The effect of the rear ride height becomes more nonlinear as the front ground clearance decreases. Figure 2.12 illustrates the effects of the yaw angle on the pitch moment. The yaw has mostly a linear effect with no rear travel, but at increased rear travels, the effect of the yaw angle on the pitch moment becomes more nonlinear especially with lower front ground clearances.

2.6 Conclusion

Current industry standard mathematical models (for vehicle dynamics simulations) or aerodynamic characteristics are unable to capture the additional nonlinear aerodynamic force and moment dependencies introduced from low front ground clearances. By implementing a dual range front ground clearance model as described in this paper, the aerodynamic model accurately fits the quasi steady state wind tunnel data.

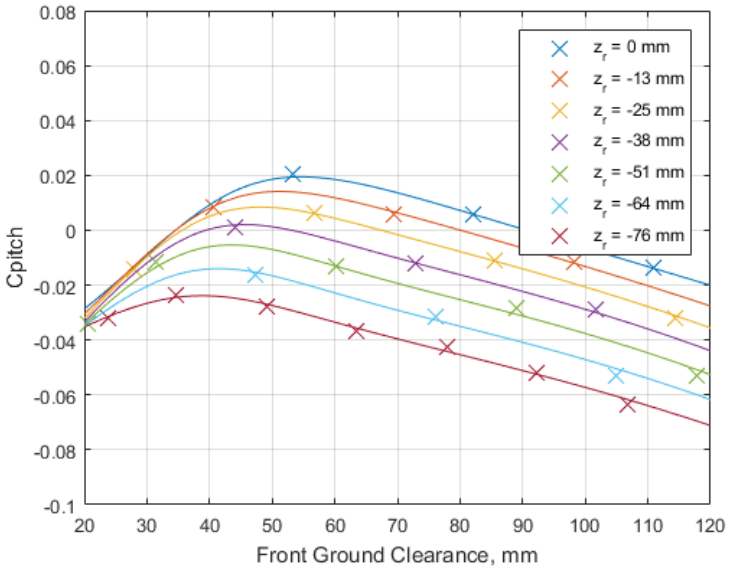

Figure 2.8: Surface fit results at 0 degrees of yaw

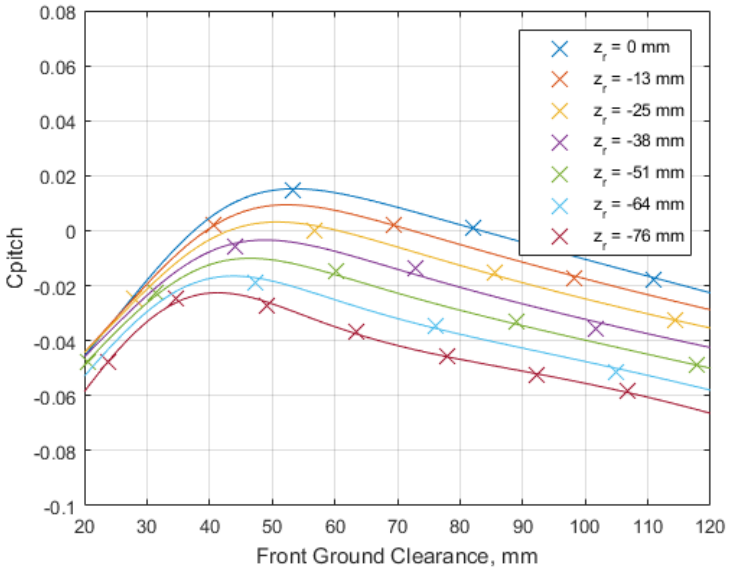

Figure 2.9: Surface fit results at 2 degrees of yaw

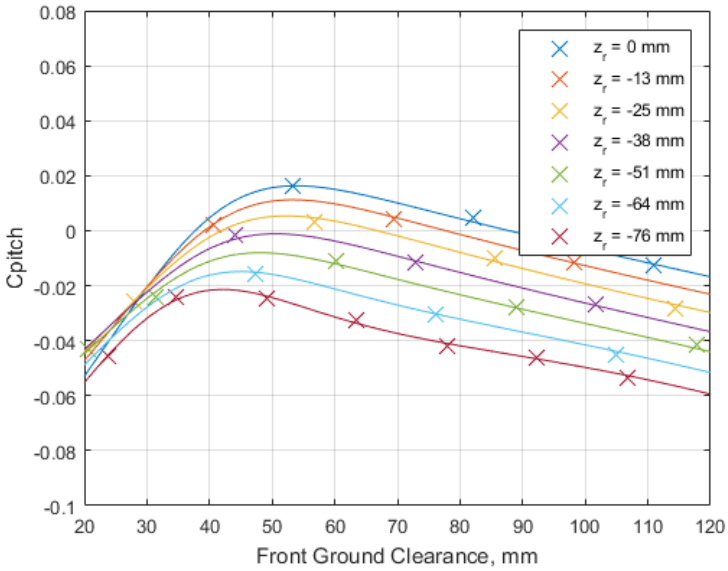

Figure 2.10: Surface fit results at 3 degrees of yaw

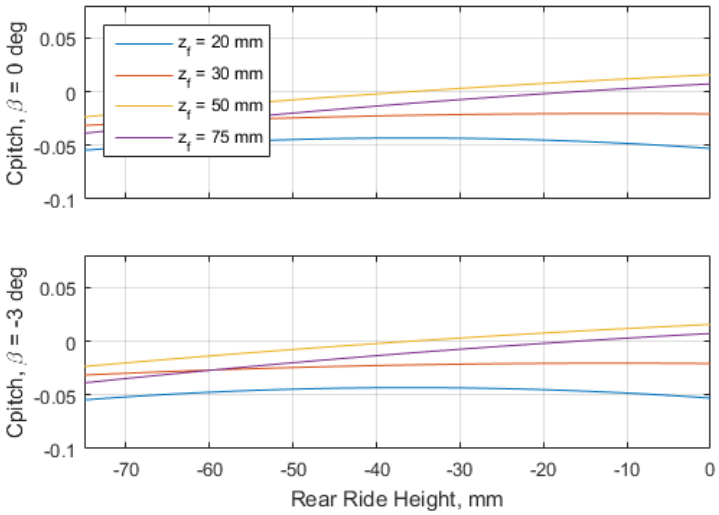

Figure 2.11: Model Results at two different yaw angles plotted against rear ride height; Top: Yaw angle of 0^o; Bottom: Yaw angle of -3^o

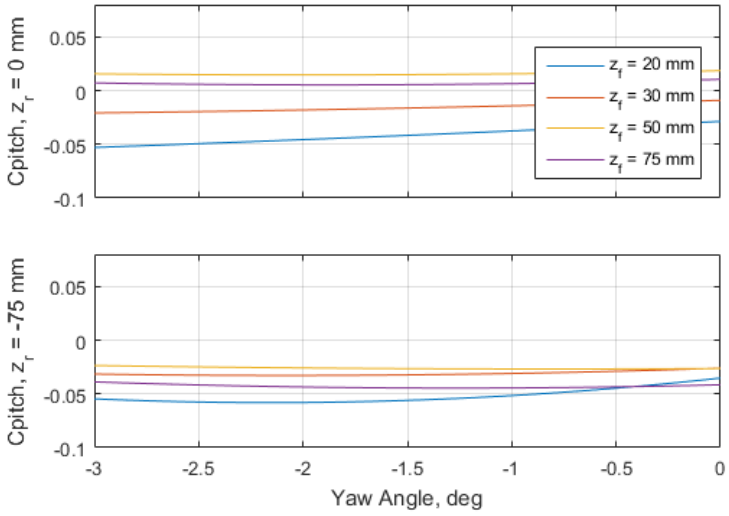

Figure 2.12: Model Results at two different rear ride heights plotted against yaw angle; Top: Rear ride height of 0 mm; Bottom: Rear ride height of -75 mm

Implementing a process, as detailed out in this paper, can reduce the parameters of the original mathematical model which decreases both the model complexity and the required amount of wind tunnel data. This quasi steady state aerodynamic model and model reduction procedure is a systematic method to develop an accurate model from wind tunnel data while reducing wind tunnel testing time and cost.

REFERENCES

[1] AeroDyn Wind Tunnel. *AeroDyn Wind Tunnel: Pricing*, 2014 (accessed June 7, 2015). http://www.aerodynwindtunnel.com/Pricing.php.

[2] Jeffery P. Chrstos. *Use of vehicle dynamics modeling to quantify race car handling behavior*. PhD thesis, Ohio State University, 2001.

[3] Fereydoon Diba, Ahmad Barari, and Ebrahim Esmailzadeh. Handling and safety enhancement of race cars using active aerodynamic systems. *Vehicle System Dynamics: International Journal of Vehicle Mechanics and Mobility*, 59(9):1171–1190, 2014.

[4] J. A. Dixon. Linear and non-linear steady state vehicle handling. *Proc Instn Mech Engrs*, 202(D3):173–186, 1988.

[5] J. A. Dominy and R. G. Dominy. Aerodynamic influences on the performance of the grand prix racing car. *Proc Instn Mech Engrs*, 198D(7):87–93, 1984.

[6] R. G. Dominy. Aerodynamics of grand prix cars. *Proc Instn Mech Engrs*, 206:267–274, 1992.

[7] Carlo Doniselli, Giampiero Mastinu, and Massimiliano Gobbi. Aerodynamic effects on ride comfort and road holding of automobiles. *Vehicle System Dynamics*, 25:S1:99–125, 1996.

[8] W. Earl Hall and Narendra K. Gupta. System identification for nonlinear aerodynamic flight regimes. *Journal of Spacecraft and Rockets*, 14(2):73–80, 1977.

[9] G. J. Heydinger, M. K. Salaani, W. R. Garrott, and P. A. Grygier. Vehicle dynamics modeling for the national advanced driving simulator. *Proc IMechE Part D: J Automobile Engineering*, 216:307–318, 2002.

[10] Wolf-Heinrich Hucho. *Aerodynamics of Road Vehicles: From Fluid Mechanics to Vehicle Engineering*. Bentley Publishers, Cambridge, Massachusetts, 1998.

[11] J. Katz. *Race Car Aerodynamics: Designing for Speed*. SAE International, 1995.

[12] Drew Landman, James Simpson, Brian Hall, and Tim Sumner. Use of designed experiments in wind tunnel testing of performance automobiles. *SAE Technical Paper*, 2002-01-3313, 2002.

[13] William F. Milliken and Douglas L. Milliken. *Race Car Vehicle Dynamics*. Society of Automotive Engineers, Inc., 1995.

[14] John Roy and Drew Landman. Aerodynamic characterization of a sportscar prototype racecar using design of experiments in a wind tunnel test. *SAE Technical Paper*, 2006-01-3621, 2006.

[15] Mohamed Kamel Salaani. *Development and validation of a vehicle model for the National Advanced Driving Simulator*. PhD thesis, Ohio State University, 1996.

[16] Windshear Inc. Private communication with Brian Nelson, General Manager, Windshear Inc., Concord, NC, USA, June 2015.

CHAPTER 3: (PAPER 2) SYSTEMATIC REDUCED ORDER MODEL DEVELOPMENT OF A PITCHING NACA0012 AIRFOIL

3.1 Introduction

Transient aerodynamic modeling is important for predicting and controlling the behavior of bodies with significant aerodynamic forces and moments. Quick computation of these aerodynamic forces is required for predicting the external forces acting on these bodies in sub real-time for use in both controls, and software and hardware in the loop applications. Computational fluid dynamics (CFD) simulations can predict the transient forces and moments [29, 1, 20, 30, 31, 24]; however, these simulations cannot be conducted in real time with today's technology. Thus, the need to create reduced order models (ROMs) from the CFD simulation results is desired. This paper presents the systematic development of simple, differential equation based ROMs to predict the aerodynamic force and moment coefficients of a 2D pitching NACA0012 airfoil.

The fundamentals of transient aerodynamic analysis have been theorized by Theodorsen [28] for a flat plate in pitching and plunging motion. This theory revealed that these transient effects are not only a function of the added mass, but also a function of circulatory effects due to the vortex shedding. Early models of the lift and pitch moment of a pitching flat plate were developed by Theodorsen [28] to capture these effects. Transient aerodynamic experimental studies have been carried out as well to further reveal the transient effects on a pitch and/or plunging airfoil [16, 22]. These studies presented lift, drag and pitch moment measurements at different pitching frequencies and amplitudes. Hysteresis in each of the aerodynamic forces and moments can be seen in the data supporting Theodorsen's theoretical work on the effects of transient

aerodynamics.

Many CFD studies have also been conducted to model and better understand the phenomena of the pitching airfoil aerodynamics. These CFD studies, ranging from unsteady Reynolds-Averaged Navier-Stokes simulation (URANS) [29, 1, 20, 30, 31] to direct numerical simulation (DNS) [24] approaches, were able to reproduce experimental data and provide physical insight into the flow characteristics that cause the transient aerodynamic effects. These CFD methods correlated well with experimental data but had significantly long run times.

Since Theodorsen's research, many ROMs of a transient body have been developed and are well described in review papers of Lucia et al.[21] and Ghoreyshi et al. [7] including ROM types such as Volterra series representations, surrogate based models, indical response functions, and Fourier based models. Treating the pitching airfoil aerodynamics as a block box, Silva[26] and Raveh[23] both developed Volterra theory based ROMs using CFD results. Silva[26] applied the Volteraa-Wiener theory to the impulse response of a rectangular wing and developed both a linear and a nonlinear lift coefficient model. The nonlinear model differed from the linear model results indicating nonlinearites in the system model do exist. Raveh[23] expanded on the theory used by Silva by developing two different nonlinear ROMs, one based on an impulse response and the other a step response. The impulse response based model was found to be limiting because the the kernels were too sensitive to the inaccuracies in the impulse response. The step response model was accurate, but Raveh found difficulty in predicting nonlinear kernels of the ROMs and thus the predictive nature of the model was not any more robust than the linear model.

Another ROM created by Glaz et al. [10] implemented a surrogate based recurrence framework approach using Kriging surrogates to account for the nonlinearities and a recurrence methodology to account for the unsteadiness effects. Using pitch angle and heave displacement as the model inputs and taking a black box approach to identifying

the system dynamics, Glaz et al. were able to accurately model the lift and drag forces and the pitch moment resulting from simultaneous pitching and plunging motions of an airfoil. Liu et al. [19] also developed a surrogate based ROM of a pitching airfoil by implementing Kriging functions trained with CFD data. The time history of the pitching angle was used as the system inputs, and a black box approach to identify the Kriging function was implemented to generate accurate models of lift, drag, and pitch moment.

Using another black box system identification approach, the indical theory appraoch, Ghoreyshi et al. [6] developed both a linear and nonlinear ROM predicting the pitching airfoil's lift and pitch moment. The linear model was only valid for lower angles of attack and diverged from the CFD results at higher angles of attack. The nonlinear model, however, generated accurate results throughout the entire pitch angle range. Another nonlinear indical function approach was developed by Bergami et al. [4] to model lift with a two-term exponential function defined by four coefficients. Each coefficient was estimated as a function of the airfoil profile angle measured at three locations along the chord enabling the lift force to be accurately predicted for pitching airfoils of various geometries.

Additional studies relevant to the research presented in this paper are those utilizing frequency domain system identification methodologies to reveal the black box system characteristics of the pitching airfoil aerodynamics. [5, 18, 32, 15] Lisandrin et al. [18] analyzed the linearity of the lift and pitch moment to the angle of attack for a $\pm 1^o$ oscillating airfoil and discovered a strong linear relationship for lift. The pitch moment relationship was primarily linear, but third and fifth order terms were shown to exist at two orders of magnitude below the linear term.

Brunton and Rowley [5] developed a linear model for lift using a state space representation of Theodorsen's model with a Pade approximation of Theordorsen's function. The added mass and quasi static coefficients in Theodorsen's model were de-

termined empirically for each operating condition tested. Good predictive results were achieved when exercising each calibrated model about its respective operating condition.

Khalid and Akhtar [15] implemented a unique approach utilizing a van der Pol oscillator model to predict the airfoil lift in pitching, plunging, and flapping motion. Using spectral analysis, Khalid and Akhtar choose the first, second, and third harmonics to estimate the frequencies and damping terms in the van der Pol oscillator model despite the spectral response for each degree of freedom not showing relevant spectral content at all three modes. While good correlation was achieved using this nonlinear model, the translation of the spectral content into the van der Pol oscillator model was quite complex.

Recently, models for lift, drag, and pitch moment have been developed for a more complex airfoil with a flexible trailing edge. [32] Qualitative analysis of the time series data led to the use of a harmonic approach for the ROM, and the order of the model was determined ex post facto by adding successive nonlinear terms to drive down the modeling error. The study revealed that a third order model of each independent variable - angle of attack, pitch amplitude, and reduced frequency - was necessary to properly model this airfoil shape.

Many of the ROMs in literature only developed models for lift and/or pitch moment, but a few of the ROMs accurately modeled all the degrees of freedom of a pitching airfoil - lift, drag, and pitch moment [10, 19, 32]. Of these, Glaz et al. [10] and Liu et al. [19] utilized complex identification procedures without providing rational for the selection of the spatial correlation functions and basis functions used to develop their surrogate based recurrence framework models. Wolff and Seume [32] qualitatively selected their modeling approach and provided no quantitative support for this selection. Each of these researchers [10, 19, 32] also determined their model order ex post facto by analyzing combinations of modeling terms and selecting the

combination which minimizes the model error.

This research sets out to systematically develop a ROM for lift, drag, and pith moment of a pitching NACA0012 airfoil using black box, frequency domain system identification techniques to determine both the nonlinear terms of the model and the coefficients of the model structure. The model structure is selected based on the common aerodynamic added mass theory resulting in simple, second order ROMs which can be easily implemented in controller design and hardware and software in the loop applications. The advantage of this approach is the systematic, as opposed to heuristic, nature of the model development and the simplicity of each ROM.

3.2 Theory

To develop the lift, drag, and pitch moment models of the pitching airfoil, the system as a whole is treated as a single-input, multi-output (SIMO) system as represented in figure 3.1. Each system is represented by a frequency response, H_l, H_d, and H_m, characterizing the dynamics between the system input, α, and the system outputs, C_l, C_d, and C_m, respectively.

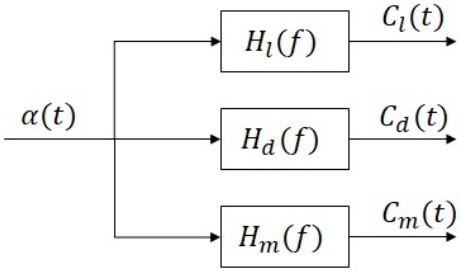

Figure 3.1: Diagram of aerodynamic forces and moments as a SIMO system

The dynamic models for lift, drag, and pitch moment are develop by analyzing two different CFD experiments. The first CFD experiment pitches the NACA0012 airfoil at a single frequency, f, and amplitude, A. Spectral analysis of these results reveal the linearity of each system. If the spectral content of the system output only contains the frequency of the system input, the system is known to be linear. If the

spectral content of the output contains frequencies in multiples of the input frequency, f, the system in known to be nonlinear. For example, if the output contains spectral content only at $2f$, the system is known to be bilinear, or if the output contains spectral content at $3f$, the system is known to be trilinear. [2]

The spectral content of each system output is evaluated using the power spectral density (PSD), S_{yy}, as

$$S_{yy}(f) = \frac{1}{T} E\big[Y^*(f)Y(f)\big] \tag{3.1}$$

where y is the generic term for each output of the SIMO system, C_l, C_d, and C_m. T is the length of the signal to be transformed, $Y(f)$ is the generic finite Fourier transform for each output signal, and the * operator denotes the complex conjugate.

Once the linearity of each system is assessed, the dynamic models for each system can be determined. This requires conducting a second CFD experiment in which the angle of attack of the airfoil is perturbed by a normally distributed, zero mean, and stationary band-limited white nose (BLWN) signal. The frequency response function for each system is computed from these results, and model coefficients are extracted by fitting the system transfer function to the frequency response.

The computation of the frequency response for lift, drag, and pitch moment relative to the angle of attack is dependent on the linearity of each of the system. Later in this paper, it is shown that both lift and pitch moment coefficients have a strongly linear relationship to α, while the drag coefficient is shown to have bilinear relationship to α. Determining the frequency response of the each linear system, generically $H(f)$, is straightforward and can be calculated as:

$$H(f) = \frac{S_{xy}(f)}{S_{xx}(f)} \tag{3.2}$$

where x is the system input which is equivalent to α for linear systems. $S_{xy}(f)$ is the cross spectral density and S_{xx} is the auto spectral density of the input computed

as:

$$S_{xy}(f) = \frac{1}{T} E\big[X^*(f)Y(f)\big] \tag{3.3}$$

$$S_{xx}(f) = \frac{1}{T} E\big[X^*(f)X(f)\big] \tag{3.4}$$

where $X(f)$ is the finite Fourier transform of the system input. For each frequency response, the coherence function, γ_{xy}^2, is also computed to evaluate the model linearity across the frequency range of interest. The coherence function is calculated as:

$$\gamma_{xy}^2(f) = \frac{|S_{xy}(f)|^2}{S_{xx}(f)S_{yy}(f)} \tag{3.5}$$

Since drag is observed to be a bilinear system, the structure of the model for drag must be revisited. Instead of representing the drag model as a single nonlinear system, the bilinear system model can be represented as a squarer operation preceding a linear system as shown in figure 3.2

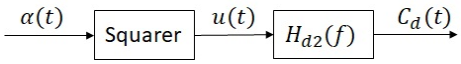

Figure 3.2: Diagram of bilinear system with squarer preceding a linear system

where $u(t) = \alpha(t)^2$ and H_{d2} is a linear system. The frequency response, H_{d2} can be computed similarly to H_l, and H_m when treating the system input x equal to u or α^2.

In this approach, the structure of each ROM must be selected to generate the transfer function to fit to the frequency response. The added mass theory reveals a second order system can model the inertial and viscous forces acting on a transient body in a fluid [11]; thus, the linear systems, H_l, H_{d2}, and H_m, are represented as a second order model. While Thoedorsen's theory indicates there are quasi static effects that could result in higher order dynamics in the lift of a pitching flat plate, the linearity study will be used to determine if any higher order dynamics significantly

contribute to the system response of the pitching airfoil. The following model is proposed for each linear system:

$$\Delta y(t) = C_{3y}\ddot{x}(t) + C_{2y}\dot{x}(t) + C_{1y}x(t) \tag{3.6}$$

where $\Delta y(t) = y(t) - C_{y0}$, and C_{y0} is the static aerodynamic coefficient value at 0^o angle of attack determined from a static equilibrium CFD experiment. Taking the Laplace Transform of the previous model and setting the initial conditions to 0, $x(t) = x'(t) = 0$, yields a transfer function with the same coefficients as the ROM.

$$\frac{\Delta Y(s)}{X(s)} = C_{3y}s^2 + C_{2y}s + C_{1y} \tag{3.7}$$

The coefficients for each model are determined by fitting equation (3.7) to the frequency response function over the frequency range of interest using Levy's theory of complex curve fitting [17].

3.3 CFD Setup

Transient CFD simulations of a pitching NACA0012 airfoil are conducted using a finite volume method commercial software package, STAR-CCM+ v11.04.010. To ensure simulation fidelity, no turbulence model is used; thus, the Navier Stokes equation is directly solved using an implicit unsteady solver at each time step. The airfoil has a chord length, c, of 0.15 m, and the freestream velocity, U, was chosen to be 14 m/s to result in a Reynolds number of 1.35x10^5. The simulation is conducted using a segregated flow solver with a velocity under-relaxation factor of 0.8 and a pressure under-relaxation factor of 0.2. After completing a convergence study on both the time step and grid size described later in this paper, the time step is 5x10^{-5} s and the grid size nearest to the airfoil is 3x10^{-4} m.

To achieve the transient analysis in the CFD simulation, an overset mesh is used to prescribe the pitching motion to the airfoil and surrounding mesh; thus, both

the airfoil and overset mesh oscillate together. The overset, or Chimera, method allows for the generation of independent meshes for various components present in a computational domain and the connection of these various domains to obtain a single universal solution [12]. The main advantage of the Chimera mesh with regard to moving bodies is its ability to treat a mesh region as a rigid body and update it from one time step to the next while still maintaining a good solution. The overset mesh moves over a background mesh spanning the entire computational domain, and the two regions are coupled at the outer boundaries of the overset mesh. The coupling of regions only affects the cells in the vicinity of the interface, and this effect can be minimized by maintaining a reasonable distance between the interface and the bodies of interest.

The overset mesh consists of a wedge shaped finer resolution mesh, shown in figure 3.3, capturing the complete wake in the mesh at every pitch angle studied. Directly surrounding the airfoil, 8 total prismatic shaped prism layers are used to capture the smaller scale near wall turbulence. Surrounding the prism layers, isotropic, polygonal shaped mesh cells are applied with a cell size that increases as the distance from the airfoil and wake regions increase. The other mesh in figure 3.3 is the background mesh composed of isotropic, polygonal shaped mesh cells which remain stationary throughout the simulation. The background mesh cells are sized to be similar to the mesh cell size at the boundary of the overset region throughout its range of motion.

The boundaries of the 2-D background region consist of a symmetry plane for both the top and bottom edges as well as a velocity inlet on the left edge and a pressure outlet on the right edge. The airfoil boundary, located within the overset region, is defined with a zero gradient condition. The airfoil is positioned $10c$ downstream of the inlet, $40c$ upstream of the outlet, and $20c$ from the top and bottom boundaries.

The Navier Stokes equation is solved directly; thus, the sizes of the mesh cells and time step must be carefully selected to ensure the time and length scales are resolved.

Figure 3.3: Overset mesh

A grid independence study using four grid sizes, *Grid*1, *Grid*2, *Grid*3, and *Grid*4, is conducted to determine the grid size effects. The corresponding base size of the mesh nearest the airfoil for each grid size is 1.5x10^{-4} m, 2x10^{-4} m, 3x10^{-4} m, and 4x10^{-4} m, respectively. *Grid*1, *Grid*2, and *Grid*3 all yield similar results, while the results of *Grid*4 diverges from the others. Since *Grid*3 is courser than *Grid*1 and *Grid*2, it is selected as the final mesh to minimize the computation time resulting in the mesh nearest the airfoil having a base size of 3x10^{-4} m. This mesh slowly grows outward to a size of 6x10^{-3} m near the overset region's boundaries resulting in about 0.65 million cells in the overset mesh. The background mesh size is also 6x10^{-3} m, resulting in about 3.2 million cells in the background mesh. To ensure that the small scales are being resolved, the results of the CFD simulation are later evaluated to find the first near wall prism layer thickness to be about 1.6 times the size of the local Kolmogorov length scale.

A time step independence study is also conducted to ensure the small time scales are being resolved while still maintaining computational efficiency. Three time steps are tested: $\Delta t_1 = 2.5x10^{-5}s$, $\Delta t_2 = 5x10^{-5}s$, and $\Delta t_3 = 1x10^{-4}s$. The results from the simulations with Δt_1 and Δt_2 produce similar results, but the result from the simulation with the largest step size, Δt_3 produces differing results. To minimize

computation time while maintaining accurate results, the time step selected is 5x10^{-5} s. Post simulation analysis shows that the selected time step is about 4.9 times the Kolmogorov time scale. An implicit solver is also implemented with 13 inner iterations to converge each residual - continuity, X-momentum, and Y-momentum - within each time step, and each residual is reduced by about three orders of magnitude as it converges.

Prior to executing each of the two CFD simulations used to create the ROMs, the CFD simulations are initially ran to achieve equilibrium of the static airfoil at a 0^o pitch angle. The static values for each aerodynamic coefficient, C_{l0}, C_{d0}, and C_{m0}, are determined from this equilibrium simulation.

The first CFD simulation consists of a single frequency pitching motion applied to the airfoil with the center of oscillation at a quarter chord and the motion defined by

$$\alpha(t) = A\sin(2\pi ft) \tag{3.8}$$

The airfoil is rotated with a frequency of 1.5 Hz and an oscillation amplitude of +/- 6^o for five cycles. An example of the first second of the input signal, α, is in figure 3.4a.

The second CFD simulation applies a pitching motion about the quarter chord position of the airfoil with the angle of attack driven by a BLWN signal. The BLWN signal is created with a cutoff frequency of 100 Hz using a 4 pole Butterworth filter and designed be normally distributed, zero mean, and stationary with a peak amplitude of 6^o. The simulation using the BLWN signal is conducted for 4 seconds to ensure the frequency content can be resolved down to 1 Hz with adequate data averaging when computing the PSDs and frequency response functions. An example of the first second of this input signal, α, is in figure 3.4b

For each CFD study, the angle of attack and the aerodynamic coefficients of lift, drag, and pitch moment are recorded to develop the models.

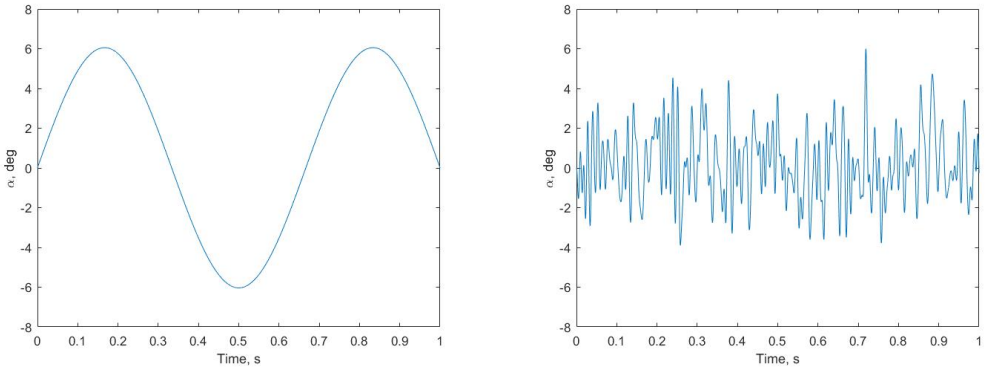

(a) (b)

Figure 3.4: Angle of attack input signals for each CFD experiment used in the system identification process; (a) Single frequency sine wave input signal, 1.5 Hz; (b) BLWN input signal

3.4 ROM Development

The development of the ROMs is completed in two steps. First, the results from the single pitching frequency CFD simulation are analyzed to determine the system linearity. Second, the frequency response functions for each system are computed from the results of the BLWN CFD simulation and fit to the transfer function in equation (3.7) to determine the model coefficients.

3.4.1 Model Linearity

To determine the ROM linearity, the PSD of each aerodynamic coefficient resulting from the single frequency CFD simulation is computed using a single rectangular window with a length spanning all 5 periods. This is the equivalent of 66,666 samples or 3.333 s, and with a sampling rate of 20,000 Hz, the 5 cycle window yields a PSD with a frequency resolution of 0.3 Hz. Prior to computing the PSDs, each coefficient is offset by its static value to remove any spectral content at 0 Hz. The resulting PSDs are in figure 3.5.

The PSD of the lift coefficient reveals spectral content at 1.5 Hz, the same as the input frequency, indicating a linear relationship between α and C_l. The higher

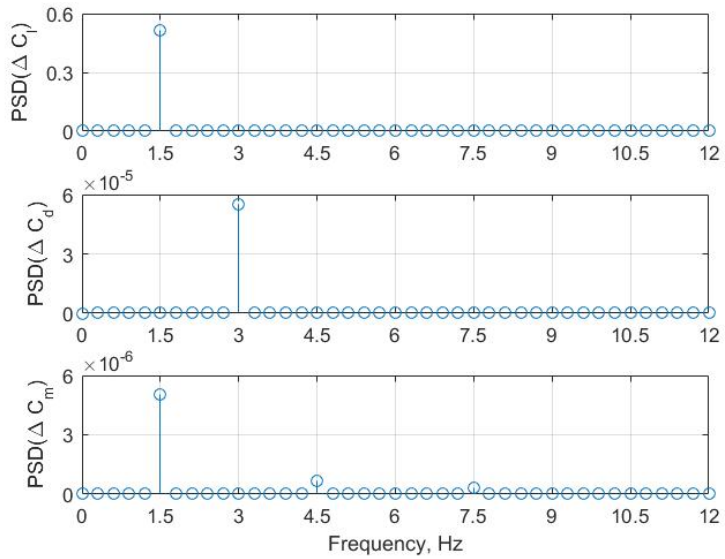

Figure 3.5: Power spectral density of aerodynamic coefficients from the single pitching frequency CFD simulation; Top: ΔC_l; Middle: ΔC_d; Bottom: ΔC_m

order dynamics in Therodorsen's equation for a pitching flat plate are not seen in the results of the pitching NACA0012 airfoil for the frequency range studied. This linear relationship between α and C_l observed in this study is also consistent with the results from Lisandrin et al. [18] of a pitching NACA64A010 airfoil.

The PSD of the drag coefficient shows the spectral content of the drag signal existing at 3 Hz, twice that of the input frequency. This indicates a quadratic relationship between α and C_d. The PSD of the pitch moment reveals the majority of the spectral content at 1.5 Hz; however, there is additional content with lower magnitudes at 4.5 Hz and 7.5 Hz, 3 and 5 times the input frequency, also consistent with earlier findings by Lisandrin et al. [18] . The magnitude of the higher order harmonics are much smaller than the magnitude of the frequency content at 1.5 Hz; thus, the pitch moment is determined to have a primarily linear relationship between α and C_m.

3.4.2 Model Coeffeicients

Based on the linearity analysis results, the aerodynamic system can be modeled as a SIMO system with linear system representations for lift and pitch moment, and a bilinear system representation for drag as illustrated in figure 3.6. In this model architecture, each frequency response, H_l, H_{d2}, and H_m can be treated as linear system.

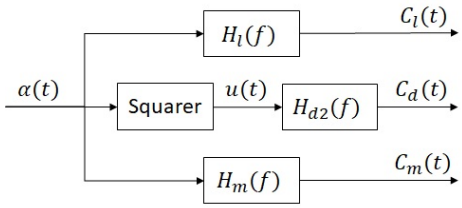

Figure 3.6: Diagram of the aerodynamic coefficient model

The frequency response functions are calculated from the 4 second BLWN simulation using a Hamming window with a length of 20,000 samples or 1 second, for a frequency resolution of 1 Hz. The windows overlap by 50% allowing for 7 windows to be averaged to smooth the frequency response. The coherence function is calculated with the same windowing. The magnitude, $|H(f)|$, and phase, $\angle(H(f))$ of the frequency response function and the coherence function are plotted for H_l, H_{d2}, and H_m in figure 3.7 to figure 3.9. These functions are studied across the frequency range of interest spanning 1 Hz, the lowest frequency resolution, to 100 Hz, the cutoff of the BLWN input signal driving α. The coefficients of the ROM, equation (3.6), are extracted by fitting the transfer functions, equation (3.7), to the frequency response. The resulting transfer function for each system is overlaid with the frequency response function in figure 3.7 to figure 3.9.

3.4.2.1 Lift

The frequency response of the lift coefficient is shown to have an increasing magnitude across the frequency range of interest as expected from the theoretical second

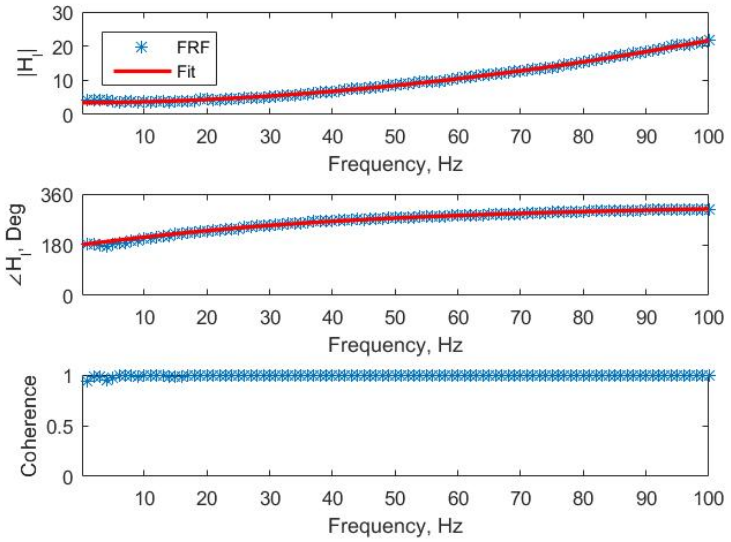

Figure 3.7: Frequency response and transfer function fit for H_l; Top: Magnitude; Middle: Phase angle; Bottom: Coherence function

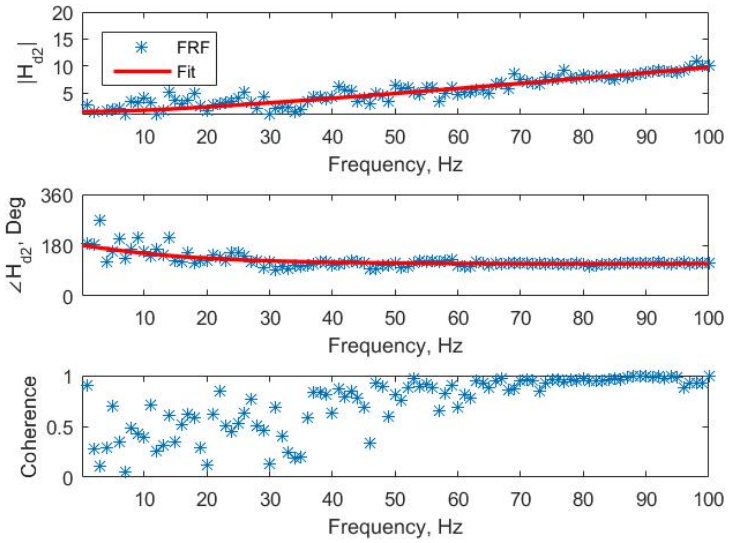

Figure 3.8: Frequency response and transfer function fit for H_{d2}; Top: Magnitude; Middle: Phase angle; Bottom: Coherence function

order model structure. The coherence function for the lift coefficient is near 1 for almost the entire frequency range except at frequencies below 5 Hz, where the coherence function still remains above 0.9. This further supports the existence of a linear relationship between α and C_l. The second order transfer function fits the

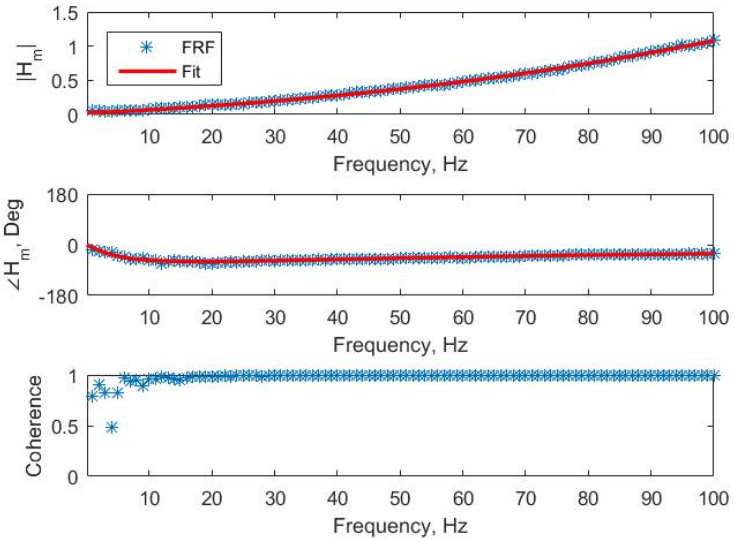

Figure 3.9: Frequency response and transfer function fit for H_m; Top: Magnitude; Middle: Phase angle; Bottom: Coherence function

frequency response of system well also supporting the selection of this model order. The resulting ROM for the lift model is:

$$\Delta C_l = -4.1919x10^{-05}\ddot{\alpha} - 0.0272\dot{\alpha} - 3.4810\alpha \tag{3.9}$$

3.4.2.2 Drag

While the frequency response of the drag coefficient shows the expected increasing magnitude across the frequency range, it is not as smooth as that of the lift coefficient. The coherence of the drag coefficient is also relatively low below 65 Hz. Above 65 Hz, the coherence function remains above 0.8, however. The linearity analysis shows a strong linear trend between drag and α^2, so the low coherence is likely attributed to a low signal-to-noise ratio rather than additional nonlinearities. Spurious numerical noise is inevitable in CFD predictions [8] which occurs because of the discrete representation of continuous transport equations, truncation of the higher order terms, round-off errors, incomplete convergence of iterative processes, and the use of adaptive numerical algorithms [25, 9]. However, such numerical noise normally

causes high frequency low amplitude waves in numerical calculations and can cause a drag variation on the order of 0.02 to 0.1 count [9]; Roy et al.[25] indicated that the numerical noise can cause 5% error in CFD predictions of drag.

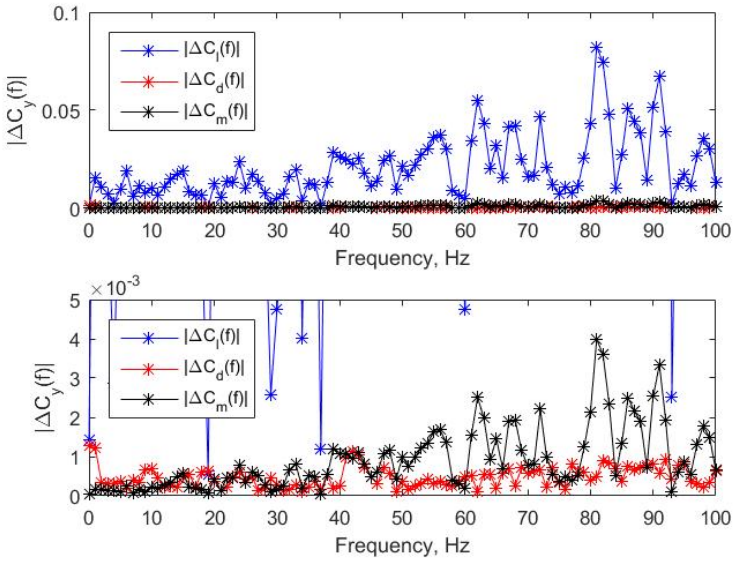

Figure 3.10: Finite Fourier transform of each system output, ΔC_l, ΔC_d, and ΔC_m; Top: Larger ΔC_y scale; Bottom: Smaller ΔC_y scale

An evaluation of the signal-to-noise ratio is beyond the scope of the current paper. However, the magnitude of the frequency content for each output signal can be assessed by analyzing the Fourier transform of these signals as displayed in figure 3.10. At all frequencies, the magnitude of the drag frequency content is significantly lower than that of the lift. The magnitude of the drag frequency content is also shown to slightly increase as the frequency increases. This is consistent with the postulation that the lower coherence at the lower frequencies is attributed to a low signal-to-noise ratio. However, since discretization or truncation errors normally impact the higher frequency contents, this discrepancy is probably due to a lack of convergence at the low frequency or, most probably, is an artifact of the overset mesh methodology. Although the overset grid offers a number of numerical advantages over the traditional unstructured grids, it cannot guarantee that the obtained numerical solution will be

globally conservative. This means that the fluxes of conserved quantities like mass and momentum when integrated over the boundary of the composite domain will not add up to zero. In incompressible flow simulations, global mass conservation is a necessary condition for the existence and uniqueness of a smooth pressure field, and such, this lack of global conservation is detrimental to the accuracy and smoothness of the computed solution [13, 27]. Additionally, the effect of overset-domain decomposition cannot be ruled out based on the findings of Benek et al.[3] who applied the Chimera approach to solving the Euler equations numerically for the transonic flow over an airfoil and found that the obtained flow fields differed significantly, depending upon whether a single domain or multiple overlapping subdomains were used. It was later realized that the anomalies in the Chimera flow field were related to a drop in the order of dissipation near artificial boundaries leading to speculations that the discrepancy resulted from the non-conservative nature of the interpolation scheme used to compute artificial boundary data [14]. However, as Keeling et al. [14] observed that no approach is completely successful in avoiding errors introduced by the transfer of values at artificial boundaries, and without knowing the magnitude of the computational noise frequency content, a valid conclusion on the signal-to-noise ratio effects on the system cannot be drawn. Subsequently, additional studies should be completed to further evaluate this hypothesis.

Assuming that the relationship can be represented as linear between C_d and α^2, the following ROM is obtained:

$$\Delta C_d = 6.2967x10^{-06}(\ddot{\alpha^2}) + 0.0141(\dot{\alpha^2}) - 1.5896\alpha^2 \tag{3.10}$$

3.4.2.3 Pitch Moment

The frequency response of the pitch moment coefficient also increases in magnitude across the frequency range as anticipated. This frequency response is much smoother

than that of the drag coefficient, and the coherence function also remains near 1 for much of the frequency range. Only at lower frequencies, below 10 Hz, does the coherence drop to values below 0.9. This is not unexpected, as the spectral analysis of the single pitching frequency CFD simulation indicated nonlinear components in the relationship between α and C_m. The magnitude of the frequency content is also very low at lower frequencies making the system identification susceptible to potential signal-to-noise ratio issues in this frequency range as well. Note that Roy et al.[25] indicated that numerical noise can cause upward of 20% error in CFD prediction of pitching moment. Since the majority of the coherence function is near 1, treating the pitch moment system as a linear system should still result in an adequate model. The second order model is again shown to represent the frequency response well, and the final ROM for the pitch moment coefficient is:

$$\Delta C_m = -2.2469x10^{-06}\ddot{\alpha} - 8.9097x10^{-04}\dot{\alpha} + 0.0289\alpha \tag{3.11}$$

3.5 ROM Results

To validate the ROMs, a third CFD experiment is conducted simulating the pitching airfoil driven by a BLWN signal uncorrelated with the BLWN signal used to develop the models. The BLWN input signal is also input into each of the ROMs to predict the lift, drag, and pitch moment coefficients, and these results are compared to the results from the CFD simulation. The results for each aerodynamic coefficient are in figure 3.11 to figure 3.13.

The ROM for lift is shown to accurately reproduce the results of the CFD simulation. This is expected as the system is shown to be highly linear and the transfer function fits the frequency response well. The ROM for drag also predicts the results of the CFD simulation well despite the uncertainty in the linearity of the system between α^2 and C_d. The drag is typically well predicted at lower angles of attack

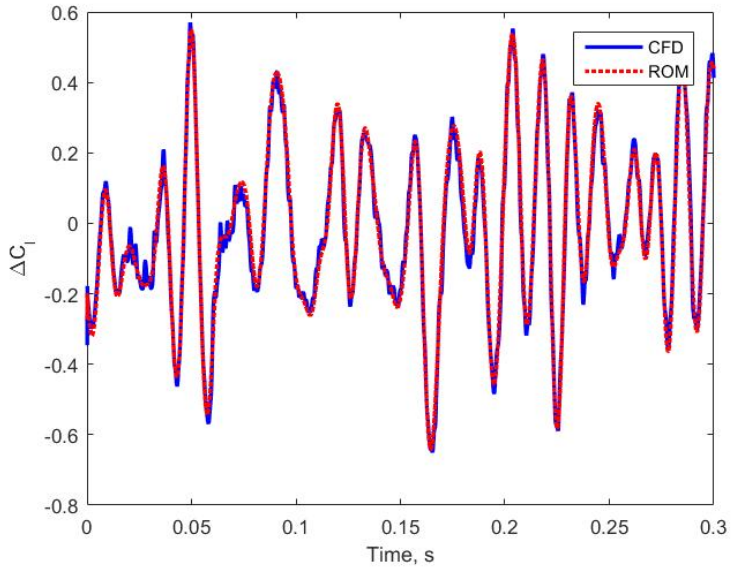

Figure 3.11: Comparison of the ROM results to CFD simulation results for C_l

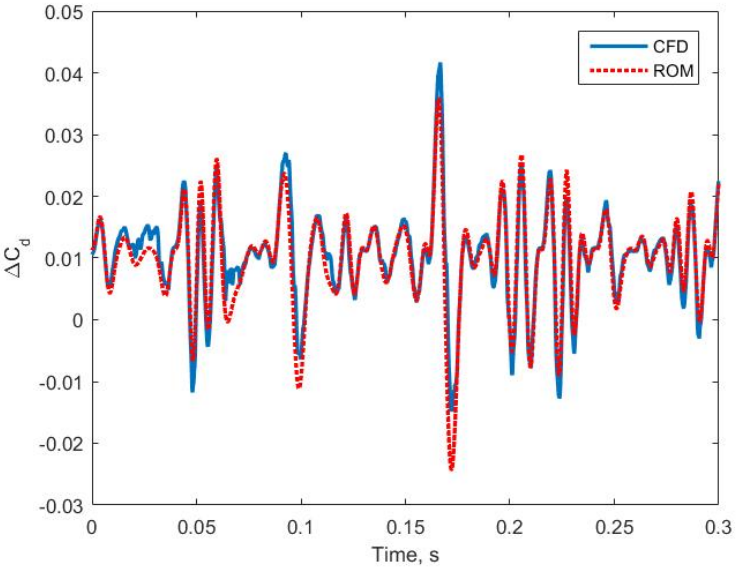

Figure 3.12: Comparison of the ROM results to CFD simulation results for C_d

amplitudes but diverges from the CFD results at higher angles of attack. The results of the pitch moment ROM also accurately reproduce the CFD pitch moment results. There is some higher frequency content in the pitch moment results that is not captured in the ROM, but this is likely due to omitting the small effects of the higher order nonlinearities in the system.

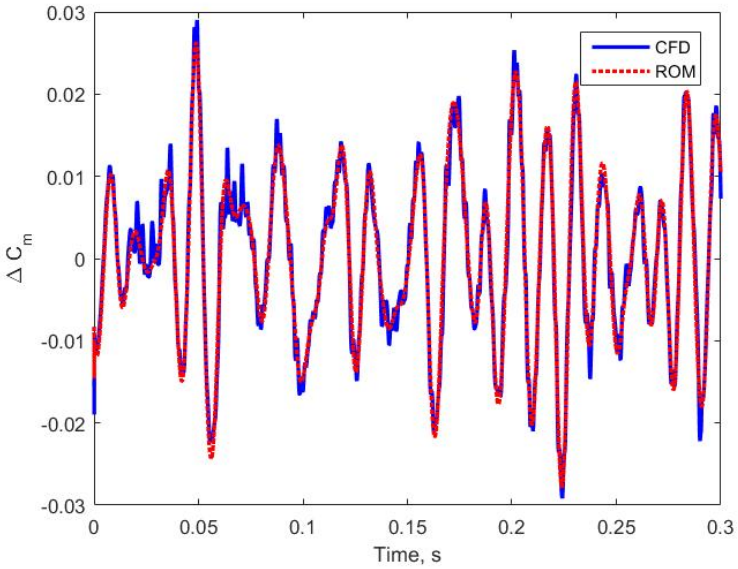

Figure 3.13: Comparison of the ROM results to CFD simulation results for C_m

3.6 Conclusion

Accurate reduced order models for a 2D pitching NACA0012 airfoil can be developed using the systematic two step procedure presented in this paper. By first identifying the linearity of the system for each aerodynamic coefficient and properly accounting for the nonlinear systems, each aerodynamic system can be modeled such that linear system identification techniques can be used to characterize each system. The lift and pitch moment coefficients are both primarily linear systems with frequency response functions well modeled by a second order system. The drag coefficient is a bilinear system, which if modeled as a linear system preceded by a squarer operation, can also yield a frequency response for the linear system well represented by a second order model.

The resulting differential equation based, second order ROMs for the lift, drag, and pitch moment coefficients are able to produce accurate results when validated against continuous random α excitations. The simplicity of the ROMs allow for extremely quick computational time and easy integration into control systems or other physical

modeling environments and allow for accurate prediction of the aerodynamic coefficients for any time varying pitch angle inputs operating within the test range. This research can be extended into different pitch angle operating ranges by implementing the same approach with either larger pitch angle oscillations or oscillations about a different mean pitch angle. Also, due to the systematic nature of this model development, this approach can be further applied to other moving aerodynamic bodies or motions along another degree of freedom. The linearity of the systems cannot be guaranteed at different pitch angles, other degrees of freedom, or on different bodies, but the nonlinear systems can be modeled as a summation of nonlinear operators preceding linear systems as implemented on the drag coefficient in this work, and the linear system identification approach can still be applied.

REFERENCES

[1] MR Amiralaei, H Alighanbari, and SM Hashemi. An investigation into the effects of unsteady parameters on the aerodynamics of a low reynolds number pitching airfoil. *Journal of Fluids and Structures*, 26(6):979–993, 2010.

[2] J.S. Bendat. *Nonlinear system analysis and identification from random data*. A Wiley-Interscience publication. Wiley, 1990.

[3] J Benek, J Steger, and F Carroll Dougherty. A flexible grid embedding technique with application to the euler equations. In *6th Computational Fluid Dynamics Conference Danvers*, number AIAA Paper 83-1944CP, page 1944, 1983.

[4] Leonardo Bergami, Mac Gaunaa, and Joachim Heinz. Indicial lift response function: an empirical relation for finite-thickness airfoils, and effects on aeroelastic simulations. *Wind Energy*, 16(5):681–693, 2013.

[5] Steven L Brunton and Clarence W Rowley. Low-dimensional state-space representations for classical unsteady aerodynamic models. In *49th AIAA Aerospace Sciences Meeting including the New Horizons Forum and Aerospace Exposition, Orlando, Florida, USA*, 2011.

[6] Mehdi Ghoreyshi, Adam Jirásek, and Russell M Cummings. Computational investigation into the use of response functions for aerodynamic-load modeling. *AIAA journal*, 50(6):1314–1327, 2012.

[7] Mehdi Ghoreyshi, Adam Jirásek, and Russell M Cummings. Reduced order unsteady aerodynamic modeling for stability and control analysis using computational fluid dynamics. *Progress in Aerospace Sciences*, 71:167–217, 2014.

[8] CA Gilkeson, VV Toropov, HM Thompson, MCT Wilson, NA Foxley, and PH Gaskell. Dealing with numerical noise in cfd-based design optimization. *Computers & Fluids*, 94:84–97, 2014.

[9] Anthony A Giunta, Vladimir Balabanov, Dan Haim, Bernard Grossman, William H Mason, Layne T Watson, and Raphael T Haftka. Multidisciplinary optimisation of a supersonic transport using design of experiments theory and response surface modelling. *The Aeronautical Journal*, 101(1008):347–356, 1997.

[10] Bryan Glaz, Li Liu, and Peretz P Friedmann. Reduced-order nonlinear unsteady aerodynamic modeling using a surrogate-based recurrence framework. *AIAA journal*, 48(10):2418–2429, 2010.

[11] Dewey H Hodges and G Alvin Pierce. *Introduction to structural dynamics and aeroelasticity*, volume 15. Cambridge University Press, 2011.

[12] Guillaume Houzeaux, Beatriz Eguzkitza, Romain Aubry, Herbert Owen, and Mariano Vázquez. A chimera method for the incompressible navier–stokes equations. *International Journal for Numerical Methods in Fluids*, 75(3):155–183, 2014.

[13] Bryan Hubbard and Hamn-Ching Chen. A chimera scheme for incompressible viscous flows with application to submarine hydrodynamics. In *Fluid Dynamics Conference*, number AIAA Paper 94-2210, page 2210. American Institute of Aeronautics and Astronautics, 1994.

[14] SL Keeling, RW Tramel, and JA Benek. A theoretical framework for chimera domain decomposition. *Advances in Flow Simulation Techniques*, 1997.

[15] Muhammad Saif Ullah Khalid and Imran Akhtar. Modeling the aerodynamic lift produced by oscillating airfoils at low reynolds number. *arXiv preprint arXiv:1502.06431*, 2014.

[16] T Lee and P Gerontakos. Investigation of flow over an oscillating airfoil. *Journal of Fluid Mechanics*, 512:313–341, 2004.

[17] EC Levy. Complex-curve fitting. *IRE transactions on automatic control*, (1):37–43, 1959.

[18] Paolo Lisandrin, Giampietro Carpentieri, and Michel Van Tooren. Investigation over CFD-based models for the identification of nonlinear unsteady aerodynamics responses. *AIAA journal*, 44(9):2043–2050, 2006.

[19] Pengyin Liu, Guohua Yu, Xiaocheng Zhu, and Zhaohui Du. Unsteady aerodynamic prediction for dynamic stall of wind turbine airfoils with the reduced order modeling. *Renewable Energy*, 69:402–409, 2014.

[20] K Lu, YH Xie, D Zhang, and JB Lan. Numerical investigations into the asymmetric effects on the aerodynamic response of a pitching airfoil. *Journal of Fluids and Structures*, 39:76–86, 2013.

[21] David J Lucia, Philip S Beran, and Walter A Silva. Reduced-order modeling: new approaches for computational physics. *Progress in Aerospace Sciences*, 40(1):51–117, 2004.

[22] KW McAlister, SL Pucci, WJ McCroskey, and LW Carr. An experimental study of dynamic stall on advanced airfoil section. Volume 2: Pressure and force data. 1982.

[23] Daniella E Raveh. Reduced-order models for nonlinear unsteady aerodynamics. *AIAA journal*, 39(8):1417–1429, 2001.

[24] Marco E Rosti, Mohammad Omidyeganeh, and Alfredo Pinelli. Direct numerical simulation of the flow around an aerofoil in ramp-up motion. *Physics of Fluids*, 28(2):025106, 2016.

[25] Christopher Roy, Carmen Heintzelman, and Samantha Roberts. Estimation of numerical error for 3d inviscid flows on cartesian grids. In *45th AIAA Aerospace Sciences Meeting and Exhibit*, page 102, 2007.

[26] Walter A Silva. Application of nonlinear systems theory to transonic unsteady aerodynamic responses. *Journal of Aircraft*, 30(5):660–668, 1993.

[27] HS Tang, S Casey Jones, and Fotis Sotiropoulos. An overset-grid method for 3d unsteady incompressible flows. *Journal of Computational Physics*, 191(2):567–600, 2003.

[28] Theodore Theodorsen and WH Mutchler. General theory of aerodynamic instability and the mechanism of flutter. 1935.

[29] J Wu Tuncer and C Wang. AlAA 89-0021 Theorectical and numerical studies of oscillating airfoils. 1990.

[30] Farooq Umar, Hossein Raza Hamdani, Sajid Raza Chaudhry, and Khalid Parvez. CFD analysis of an oscillating wing at various reduced frequencies. *International Journal for Numerical Methods in Fluids*, 59(2):173–194, 2009.

[31] Shengyi Wang, Derek B Ingham, Lin Ma, Mohamed Pourkashanian, and Zhi Tao. Numerical investigations on dynamic stall of low reynolds number flow around oscillating airfoils. *Computers & Fluids*, 39(9):1529–1541, 2010.

[32] T Wolff and JR Seume. Modeling the transient aerodynamic effects during the motion of a flexible trailing edge. In *Journal of Physics: Conference Series*, volume 753. IOP Publishing, 2016.

CHAPTER 4: (PAPER 3) REDUCED ORDER AERODYNAMIC MODEL OF A RACE VEHICLE IN PITCHING MOTION

4.1 Introduction

Modeling the transient aerodynamic forces and moments acting on a vehicle is of particular importance in the automotive modeling and simulation field of study. The automotive industry is replacing physical testing with virtual testing thus increasing the reliance on accurate vehicle simulations. The increased use of driver-in-the-loop (DiL), hardware-in-the-loop (HiL), and software-in-the-loop (SiL) testing, collectively referred to as XiL testing, as well as the need for accurate plant models for autonomous driving controllers is pushing the need for more accurate, higher fidelity vehicle models. The motorsports sector, in particular, relies on accurate, high-fidelity vehicle simulation for both XiL testing and vehicle performance predicting simulation. The vehicle aerodynamics is a significant source of forces and moments acting on the vehicle especially at higher speeds such as those seen during freeway driving and closed circuit racing. Modeling the vehicle aerodynamics accurately is necessary to develop a well correlated vehicle model. Additionally, vehicle modeling for use in XiL testing and autonomous vehicle controllers must be real-time capable. This added constraint drives a requirement for a reduced order aerodynamic model for use in automotive simulation applications. A complete CFD simulation, which could produce accurate transient results, is not a viable solution currently due to the long run times required.

Vehicle aerodynamic modeling has traditionally been limited to quasi steady state models generated from curve fitting the aerodynamic force and moment data measured in the wind tunnel with respect to the independent variables describing the vehicle orientation: front travel, rear travel, and yaw [5, 13]. These aerodynamic

models have become more advanced over the years, but they still only model the quasi steady state aerodynamic forces and moments. More recently, researchers have developed transient aerodynamic models to account for the vehicle body motion with respect to the ground due to bumps, road curvature, and vehicle cornering effects [15, 17, 10]. Previous research has shown transient vehicle body motions affect the aerodynamic forces and moments and cause them to differ from the quasi steady state forces and moments [1, 3, 8, 14].

The aerodynamic effects of a pitching vehicle were first studied by Aschwanden et al. [1] at the scale model Automotive Wind Tunnel in Emmen, Switzerland. A motion system was developed to enable the pitching and heaving of the scale model vehicle in the wind tunnel, and transient tests were performed on a 50% scale LeMans style vehicle model. The vehicle was exercised in heave at frequencies of 1, 3, 6, and 10 Hz, with amplitudes of 1, 2, and 4 mm or in pitch at a frequency of 10 Hz with a 0.5° amplitude. The data was post-processed to remove the inertial effects, and the effect on the drag and front and rear downforce was analyzed. The aerodynamic characteristics of the vehicle in transient motion were shown to significantly vary from the characteristics of the static vehicle. Pressure taps were also located along the vehicle centerline and reveled that the majority of the transient effects could be attributed to the flow along the underbody.

This research was furthered by Kawakami et al. [10] to compare the results of the experimental testing to large eddy simulation (LES) CFD analysis. A simpler Ahmed vehicle model, measuring 1044 mm in length, with no suspension or wheels was used for this study. In both the wind tunnel and CFD simulations, a vehicle was tested in pitch and heave at three frequencies, 2, 4, and 8 Hz, with amplitudes of 8 mm in heave and 0.878° and 3° amplitudes in pitch. The lift and pitch moment from the CFD and experimental results were shown to correlate well. A reduced order model was developed for the lift and pitch moment as a function of heave and pitch and

their first derivatives, but the model fitting was limited to using data from only three testing frequencies. The results from applying the reduced order model were also not published, so the accuracy of this modeling approach is unknown.

Nakashima et al. [15] and Tsubokura et al. [17] conduct LES simulations on two different shaped 1/20 scale simplified vehicle bodies without wheels undergoing a 10 Hz pitching motion with a 2° amplitude. For both body shapes, the transient aerodynamic characteristics were shown to vary from the static vehicle simulation results, and the variation in the body shape was shown to have different effects on the transient aerodynamic characteristics of the two bodies. For these particular body shapes, the differences in the rear deck lid shape resulted in differing flow fields above and behind the deck lids and thus had significant effects on the pitch moment of the vehicle. The pitch moment results from this single frequency pitching motion were fit to a second order model of pitch angle, and the differences in the transient aerodynamics of the two body shapes were shown to manifest themselves in the ROM coefficients as well. While ROMs were developed for the two different body shapes, the ROMs were never validated against any uncorrelated CFD or experimental data.

Gu et al. [8] conduct LES simulation on a pitching vehicle model composed of a 1/3 scale simplified passenger car body with wheels. The wheels remain in the same location throughout the simulation while the vehicle body pitches with respect to the ground frame at a frequency of 10 Hz and an amplitude of 2°. Differences in the drag and lift aerodynamic coefficients are seen between the static and pitching vehicle and are qualitatively similar to the previous research conducted without wheels on the vehicle. For the particular body style studied, the flow field suggests that these differences emerge from the flow directly behind and underneath the vehicle body.

Utilizing a more complex vehicle model than previous research, Nakae et al.[14] conduct LES CFD simulations on a 1/4 scale vehicle model in pitching motion. The vehicle model contains separate wheels and an engine compartment housing an engine,

a radiator with air inlets and outlets into the engine compartment, and the front suspension. An under floor tunnel is also present housing the exhaust components. The remainder of the vehicle body is a closed smoothed surface resembling a real production car. The wheels remain in a static location relative to the ground while the vehicle is pitched at 5.5 Hz with an amplitude of 1.32°. Similar to other research, the transient front, rear, and total lift is shown to vary significantly from the static vehicle aerodynamic characteristics. Flow field analysis reveals significant flow field differences in the under body of the vehicle as well as around the front wheel housing.

While many transient vehicle CFD studies employ the LES models, Kawamura and Ogawa [11] utilize a URANS approach. They conduct a heave test of a 1/5 scale simplified passenger car body in a tow tank changing the working fluid from air to water and compare the results to the URANS CFD simulation. The lift results were compared and found to correlate well. Flow analysis showed the transient lift effect was produced by the pressure change in the under body and increased as the vehicle moved closer to the ground due to the ground effect.

A few researchers also studied the impact of the transient aerodynamics on vehicle performance. In a more qualitative study, Cheng et al. [4] analyzed the results from the previous work of Nakashima et al. [15] and Tsubokura et al. [17] to conclude that the different vehicle body shapes, especially in the read deck lid area, result in different vehicle pitch stability metrics and encourage attention to the pitch stability in the design of the body shape.

A more qualitative approach is used by Aschwanden et al. [2] to study the significance of the transient aerodynamic effects on simulated cornering maneuvers of a race vehicle. By applying the transient hysteric effects of the lift discovered in their previous research [1] to a vehicle dynamics simulation, the results reveled that the transient aerodynamics had a significant effect on the predicted vehicle cornering performance.

The work presented in this paper employs URANS CFD simulations to study the effect of the vehicle pitching motion on all six aerodynamic force and moment coefficients of a full size race vehicle, specifically a 2006 NASCAR Truck. The NASCAR Truck is a race modified version of a production pickup truck raced in the NASCAR Gander Outdoors Truck Series, a series owned and operated by the National Association for Stock Car Auto Racing, popularly known as NASCAR. The Truck Series races on primarily oval shaped circuits of various distances, bank angles, and vehicle top speeds, and the trucks can see speeds up to 90 m/s (200 mph) at the fastest circuits.

The goal of this research is to produce reduced order aerodynamic models to predict the transient aerodynamic coefficients utilizing CFD simulations. The reduced order models are validated against additional CFD simulations to ensure accuracy. While previous research has developed ROMs for the lift and pitch moment of a vehicle relative to the pitch angle, to the best of the authors' knowledge, this is the first publication modeling drag as a function of vehicle pitch and validating the aerodynamic ROMs. This research also proposes a new structure for the transient ROMs to better predict the transient aerodynamic coefficients. These reduced order models, when applied in vehicle dynamics simulation, should increase the fidelity of the load predictions on the vehicle model, thereby improving the simulation's predictive capability [2]. The application of these reduce order aerodynamic models in vehicle dynamic simulation will be studied in future work.

4.2 CFD Simulation

This study utilizes a commercial CFD package (STAR-CCM+ version 13.04) to study the aerodynamic characteristics of both a static and transient vehicle. A CFD approach is chosen over an experimental approach because previous research has shown good correlation between experimental and computational results using both LES and URANS approaches [10, 11], and CFD is less costly and more read-

ily available than physical testing. CFD also allows for more insight into flow field visualization without requiring additional and even more costly testing equipment.

4.2.1 Vehicle Model

The vehicle model, illustrated in figure 4.1, is a detailed, full scale 2006 NASCAR Truck race vehicle with all radiator, ducting, and windows areas sealed. The underbody consists of all the components in the actual vehicle with the exception of the the suspension and rear axle components in close proximity to the wheels. These components are trimmed away from the wheels enabling the numerics to properly converge when applying the motion between the vehicle and the wheels. To make the truck more aerodynamically suited to race at high speeds, modifications are made to the traditional pickup truck body. The front fascia of the vehicle is extended further toward the ground, the traditional bed of the pickup truck is covered, and a spoiler is added to the rear of the truck. The vehicle geometry used in the CFD simulation positions the vehicle close to the ground plane representative of the vehicle travel on the racing circuit.

4.2.2 Simulation Experiments

This study is conducted in multiple phases. First, a static vehicle simulation is conducted with the baseline vehicle geometry at 0° pitch and compared to static wind tunnel data of the same vehicle position to verify the numerical method. Second, static vehicle simulations are conducted at four additional pitch angles, 0.25°, 0.5°, 0.75°, and 1°, to capture the quasi steady state aerodynamic coefficients and flow fields. Next, a ±0.5°, 4 Hz pitching motion is applied to the vehicle, and the aerodynamic coefficients are continuously recorded while flow field data is phase averaged at eight points throughout the pitch cycle: 0°, 0.25° upstroke, 0.5° upstroke, 0.75° upstroke, 1°, 0.75° downstroke, 0.5° downstroke, and 0.25° downstroke. Finally, band-limited white noise pitch signals are used to define the vehicle motion to characterize and

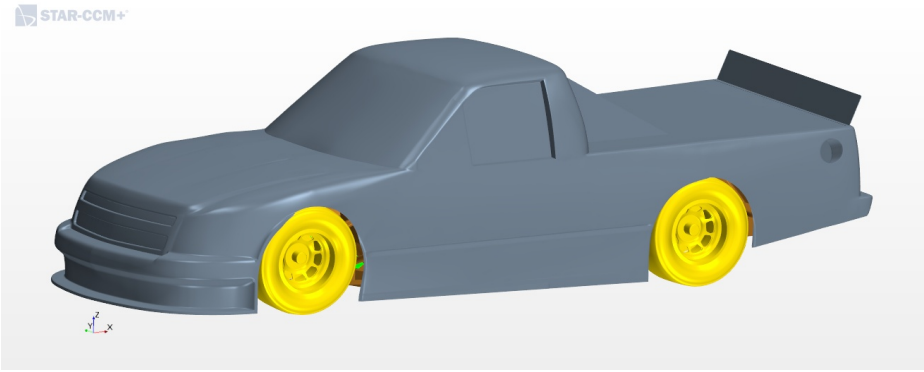

(a)

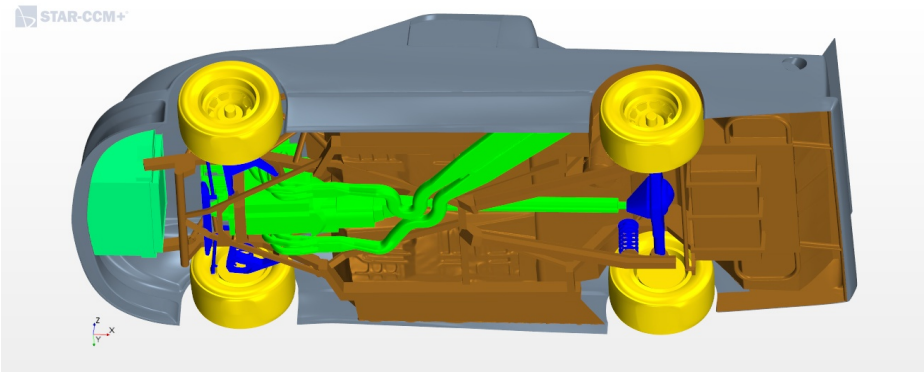

(b)

Figure 4.1: CFD vehicle model; (a) Top view; (b) Underbody

validate the transient ROMs. The simulation setup is the same for each phase of this study with the exception of the motion specifications.

4.2.3 Computation Domain

The computational domain, shown in figure 4.2, is a rectangular cuboid test section measuring 150 m (30L) long, 90 m (30W) wide, and 45 m (15H) high. The vehicle model is placed on the lower boundary of the domain, referred to as the ground plane, about 10L behind the inlet, and equidistant from the right and left boundaries of the test domain. The ground plane contains a belt section located below the vehicle measuring 12.75 m long and 10 m wide used to simulate the rolling road surface. This section begins about 2 m in front of the leading edge of the vehicle, and is centered right-to-left in the domain.

The computational domain is separated into two regions with an overset interface defined between the regions. The overset region contains the vehicle model without the wheels, and the background region contains the remainder of the domain including the wheels and the domain boundaries. The definition of the regions is illustrated in figure 4.3 and 4.4. The separate regions allow for motion to be applied to the overset region only, while keeping the test domain and wheels stationary during the transient simulations. The pitch motion is applied to the overset region, and thus the vehicle body, about the rear axle centerline.

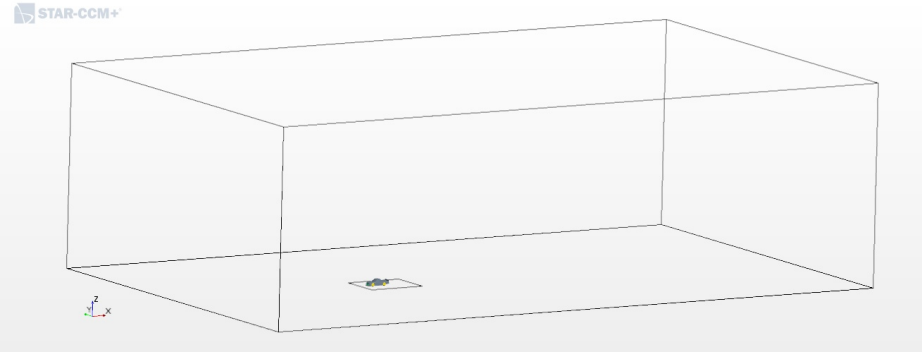

Figure 4.2: Computational domain

4.2.4 Boundary Conditions

The boundary conditions are defined in the background region to simulate the vehicle traversing the ground at 70 m/s (157 mph), a typical race circuit speed for a 2006 NASCAR Truck. A velocity inlet with a 70 m/s velocity magnitude, 1% turbulence intensity, and 10 mm turbulent length scale is applied to the upstream test domain boundary, and a pressure outlet is applied to the downstream boundary. The ground plane not included in the belt section is defined as a slip wall, and the belt section is defined with a 70 m/s tangential velocity to simulate the rolling road condition. The test domain side and top boundaries are assigned a symmetry plane boundary condition, and the wheel surfaces are all defined with a relative rotation rate of 197 rad/s to simulate their rotation at 70 m/s.

4.2.5 Mesh

The background and overset regions are meshed independently. The background region, figures 4.3a and 4.4a, is meshed with trimmer cells that slowly increase in size as the distance from the vehicle and vehicle wake increase. The belt section and wheels contains prismatic cells with a geometric growth rate to resolve the near-wall flow. The overset region, figures 4.3b and 4.4b, also contains trimmer cells which increase in size as the distance from the vehicle surfaces increase. Prismatic cells with a geometric growth rate are used on all vehicle surfaces resulting in a wall-node y^+ near or below 1 for almost all of the vehicle surface.

When the background and overset meshes are coupled using the overset interface, a hole is cut in the background mesh using the alternate hole cutting routine in STAR-CCM+ to create the final volume mesh shown in figures 4.3c, 4.4c, and 4.5. The only overlapping cells occur at the interface between the two regions and are used to interpolate values between the donor cells in the background region and the acceptor cells in the overset region. Here, the mesh cell sizes are designed to be of similar size to minimize the discretion error in the linear interpolation routine applied. The wheel boundaries in the background region are defined to maintain more active layers than prism layers, ensuring a boundary of trimmer cells around the wheels after the overset mesh hole cutting is performed. This area is of particular focus due to the close proximity between the wheels and the vehicle body shown in figure 4.5. When the motion is applied, the hole cutting routing occurs at each time step ensuring the proper interface of overlapping cells between the two regions at each position of the overset region.

In an effort to reduce run time, multiple mesh sizes were evaluated to determine the smallest amount of cells required to maintain simulation accuracy. The largest mesh size found to maintain this accuracy resulted in a cell count of 48 million in the background region, 24 million in the overset region, and 72 million cells overall.

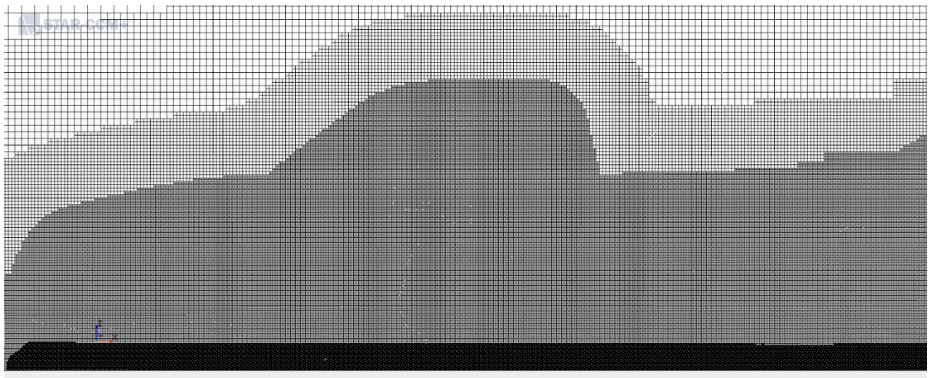

(a)

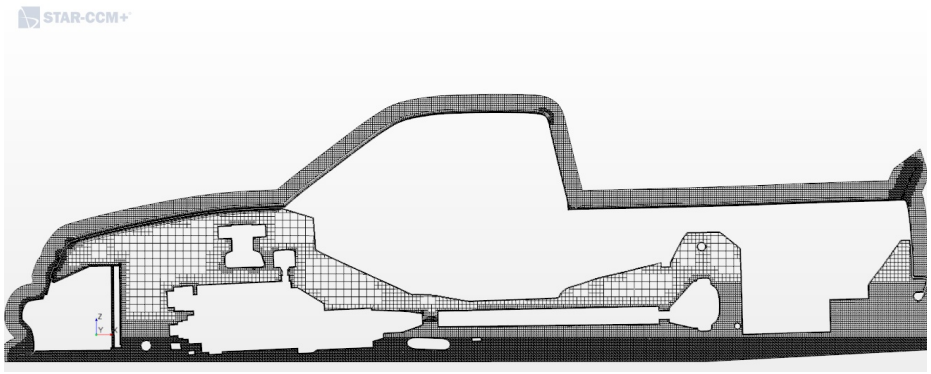

(b)

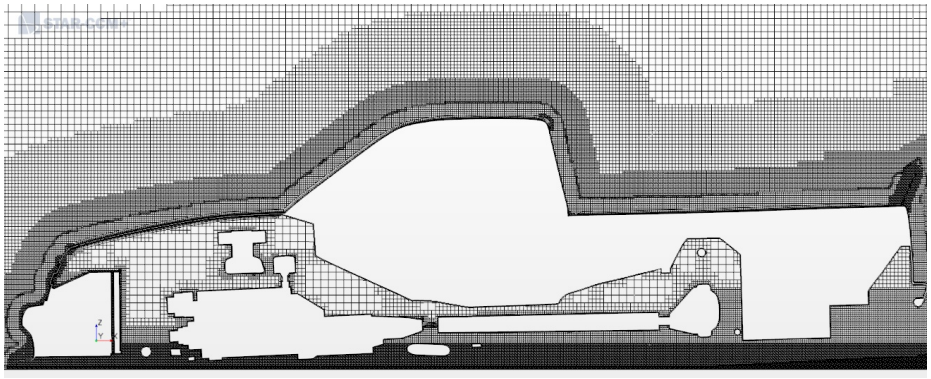

(c)

Figure 4.3: Mesh on $Y-Z$ plane at vehicle centerline; (a) Background region overset mesh; (b) Overset region overset mesh; (c) Combined region volume mesh

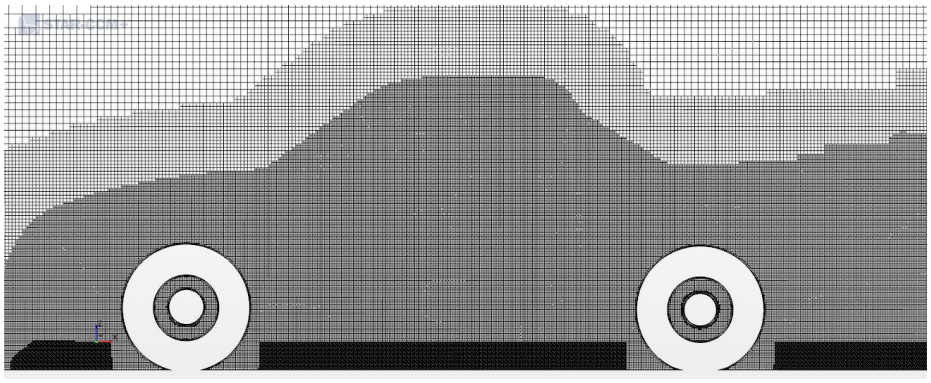

(a)

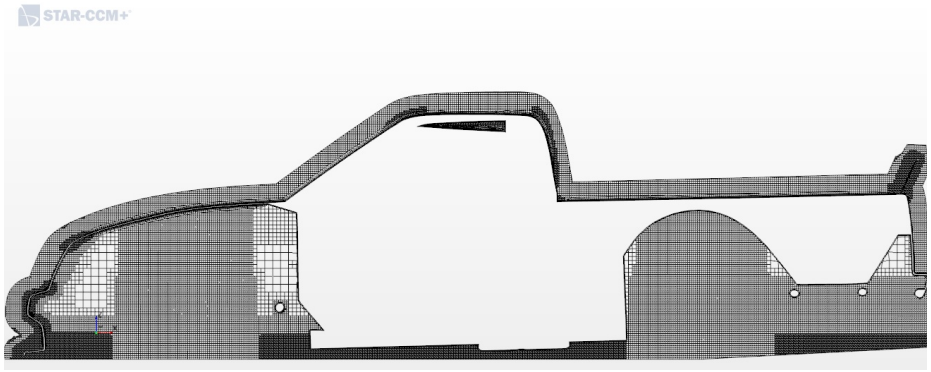

(b)

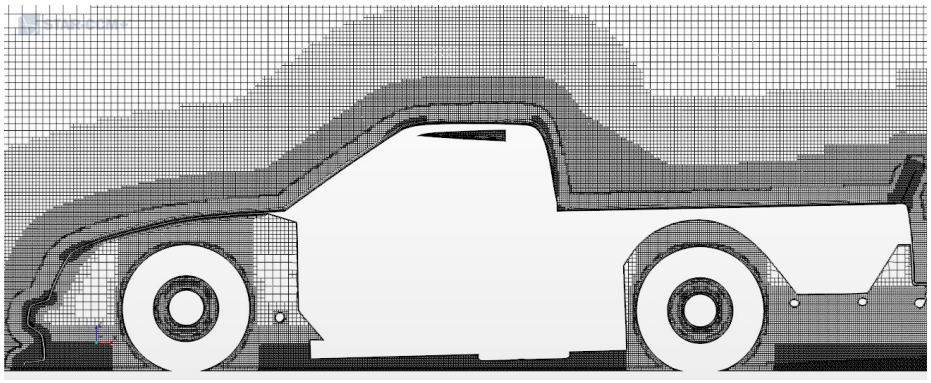

(c)

Figure 4.4: Mesh on $Y - Z$ plane at left side wheel center location; (a) Background region overset mesh; (b) Overset region overset mesh; (c) Combined region volume mesh

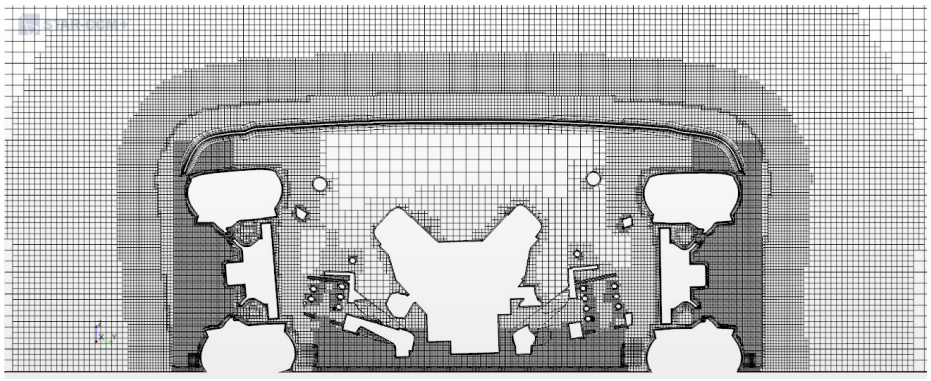

(a)

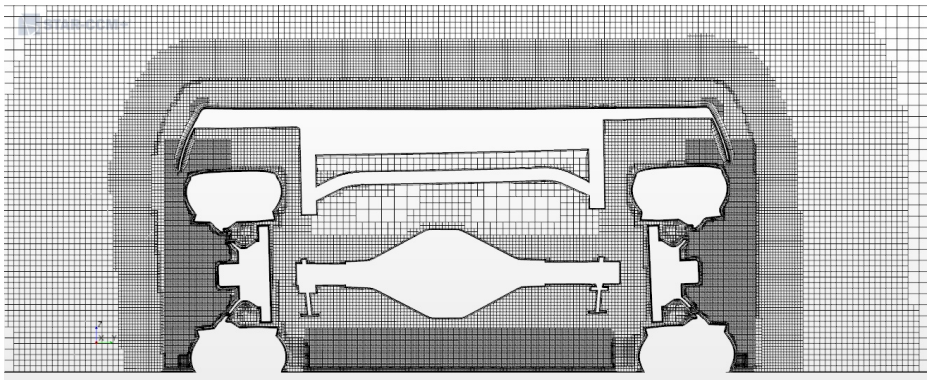

(b)

Figure 4.5: Combined region volume mesh on $X - Z$ planes; (a) Front wheel center location; (b) Rear wheel center location

4.2.6 Physics

URANS CFD simulations are chosen so the aerodynamic characteristics of a static and pitching full size vehicle model can be computed while maintaining a reasonable simulation run time. RANS has been effective for accurately predicting the aerodynamic forces on a static race vehicle [6], and URANS has shown good correlation to experimental transient data as well [11].

To initialize each simulation, the vehicle is held at 0° pitch, and a RANS simulation is first ran for 7000 iterations before switching to a URANS simulation for an additional 1 s of simulation. This ensures the residuals have converged and decreased by 2 to 5 orders of magnitude from the start of the simulation.

After this initialization at 0° pitch, URANS simulations are continued to complete

the static or transient vehicle studies. For both the RANS and URANS simulation, the SST Menter K-ω turbulence model is used with an all-y^+ wall treatment. All the STAR-CCM+ default values assigned to these physics models are used in the simulation, and no additional model coefficient modification are made.

For the initial RANS simulation, the fluid is modeled as incompressible. When the physics model is changed for the URANS simulation, the fluid is modeled as compressible and the segregated fluid temperature model is also included. This change to the physics configuration is necessary for convergence of the overset mesh simulation.

The segregated flow solver with a flux correction conservation option is applied for both the RANS and URANS simulations. For the URANS simulation, a second order implicit integration scheme with a 2e-4 s time step is used with 4 inner iterations. Prior to selecting 2e-4 s as the final time step, smaller time steps, 1e-4 s and 5e-5 s, and a lager time step, 5e-4 s, are applied to the simulation. The 2e-4 s time step and the smaller time steps all produced similar simulation results. The larger time step produced simulation results which differed from the results of the other time steps. Thus, to minimize run time, 2e-4 s is selected as the time step for use in the URANS simulations. Different inner iterations are also evaluated. Inner iterations above 4 minimally impact the residual reduction, so for run time considerations, 4 inner iterations are selected.

4.2.7 Static Vehicle Simulations

For the static vehicle simulation at 0° pitch, the initialized simulation, as described in the preceding Physics section, is simulated for an additional 1.5 s to record and average the aerodynamic coefficients and flow fields. For the other four static vehicle simulations at 0.25°, 0.5°, 0.75°, 1° of pitch, a 0.25 s duration pitch angle ramp motion is applied to the initialized simulation to move the vehicle body to the respective pitch angle which is held constant for the remainder of the simulation. The simulation is run for another 0.75 sec to allow the simulation to converge at the new pitch angle,

and then an additional 1.5 s is simulated to record and average the flow fields. The pitch angle is evaluated between 0° and 1° to emulate the travel of the vehicle body on the racing circuit.

4.2.8 Transient Vehicle Simulations

The first transient vehicle simulation applies a single frequency ±0.5°, 4 Hz pitching motion to the vehicle body. Insight into the transient aerodynamic characteristics is provided by analyzing the aerodynamic coefficients throughout the pitch cycle and the flow field around the vehicle at eight points within the pitch cycle: 0°, 0.25° upstroke, 0.5° upstroke, 0.75° upstroke, 1°, 0.75° downstroke, 0.5° downstroke, and 0.25° downstroke. Beginning with the initialized simulation at 0°, ten pitch cycles are simulated over 2.5 s. The first half of the cycle is the upstroke, peaking at 1° of pitch, and the second half of the cycle is the downstroke. The first four cycles, or 1 s, of simulation allow the transient simulation to settle, and the final six cycles, or 1.5 s, are recorded and phase averaged for the analysis. The pitching motion frequency of 4 Hz is chosen to be in the range of the pitch natural frequency of the race vehicle, and the amplitude is chose to span the same range as the static vehicle simulations which emulate the vehicle travel on the racing circuit.

The second vehicle simulation applies a 0.5° mean, 25 Hz band-limited white noise pitching motion to characterize the transient aerodynamic ROM. The simulation is run for 5 seconds, allowing 1 s for the transient simulation to settle and then recording the aerodynamic coefficients and pitch angle for the last 4 s. The band-limited white noise amplitude is scaled to ensure the maximum pitch angle does not exceed ±0.5°. Based on inertial sensor measurement from the race vehicle, the body excitation is below 15-20 Hz; thus, the pitch excitation bandwidth limit of 25 Hz captures the dynamics occurring on the race circuit.

The final vehicle simulation also applies a 0.5° mean, 25 Hz band-limited white noise pitching motion; however, this motion is uncorrelated with the pitching motion

used to characterize the ROM. This simulation is run for 2 s, and the aerodynamic coefficients and pitch angle are recorded for the final 1 s and compared with the results from the reduced order aerodynamic model for model validation purposes.

4.3 CFD Results

The aerodynamic coefficients resulting from the static vehicle 0° pitch simulation are within 5% of the experiment values for lift and drag and within 1% of the experimental percent front lift distribution thus validating the numerical setup of the simulation.

The phase averaged aerodynamic coefficients from the 4 Hz pitching motion simulation are compared to the results from the static vehicle simulations in figure 4.6. These results are qualitatively similar to other transient vehicle experimental results published in literature [1]. The transient motion simulations show large amounts of hysteresis in the aerodynamic coefficient for the lift and drag coefficients with less drag and lift being produced in the upstroke than in the downstroke. The side force and pitch moment coefficients show small variations between the upstoke and downstroke, but a clear indication of hysteresis is not seen, and nearly identical values are produced for the roll moment and pitch moment coefficients in the upstroke and downstroke.

The slope of the aerodynamic coefficient with respect to pitch angle are similar between the static and transient vehicle simulations for the drag, side force, roll moment, and yaw moment coefficients, but the slopes differ significantly for the lift and pitch moment coefficients. This indicates that any aerodynamic model developed from static vehicle data only is not only unable to predict the hysteric effects in the drag and lift coefficients but is also unable to predict the sensitivity of the lift and pitch moment coefficients to variations in pitch angle.

The flow field visualizations indicate that the primary difference between the steady and transient flow fields as well as the upstroke and downstroke flow fields occurs along

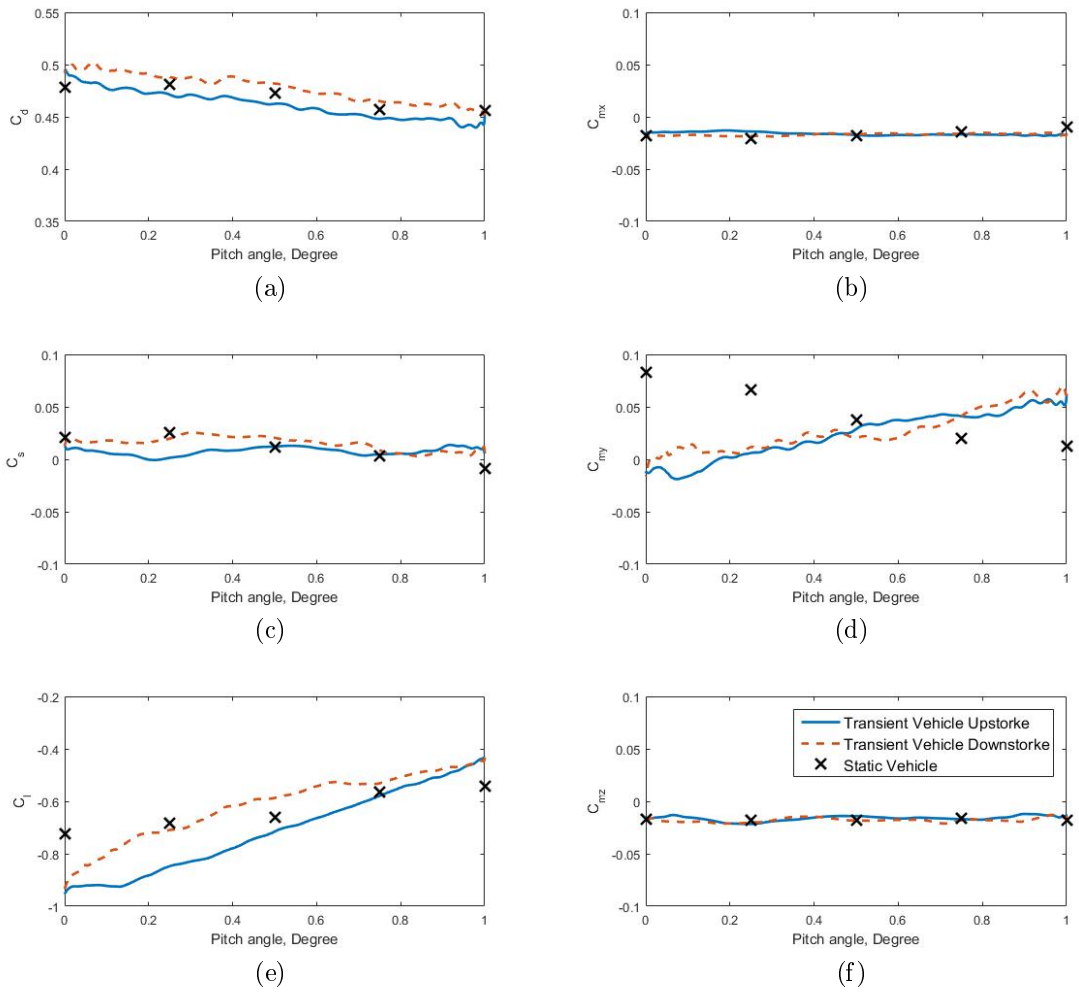

Figure 4.6: Aerodynamic coefficient comparison between the static vehicle simulations and the transient vehicle 4 Hz pitching motion simulation; (a) Drag coefficient, C_d; (b) Roll moment coefficient, C_{mx}; (c) Side Force coefficient, C_s; (d) Pitch moment coefficient, C_{my}; (e) Lift coefficient, C_l; (f)Yaw moment coefficient, C_{mz}

the underbody at the front of the vehicle. The height of the leading edge of the vehicle controls the air flow under the vehicle, and the aerodynamic coefficients change as this leading edge height changes due primarily to the air flow under the vehicle. Figures 4.7 - 4.9 contain the mean X-velocity, mean total pressure, and mean vorticity fields, respectively, captured on the vehicle centerline plane in the static vehicle simulations. These fields show the flow along the underbody in this region is generally steady.

Figures 4.10 - 4.12 show the phased averaged mean X-velocity, mean total pressure, and mean vorticity fields, respectively, captured on the vehicle centerline plane at

eight pitch angles throughout the pitch cycle in the 4 Hz pitching motion simulation. The flow along the underbody in the front of the vehicle is no longer steady once the pitching motion is applied. The flow fields not only differ from the static simulation results at the same pitch angles, but the transient flow fields also differ between the upstroke and downstroke for the same pitch angle.

The flow is close to steady in the 0° pitch angle orientation. During both the upstroke and downstroke, vortical structures begin to form in the underbody flow causing the high and low velocity and pressure variations in this region. In the upstroke, the vortical structures do not become fully developed until 0.75° and then they begin to subside when the vehicle reaches the upper inflection point of the pitching motion cycle at 1°. In the downstroke, the vortical structures form quicker than on the upstoke, and are clearly developed at 0.5°. The presence of the vortical structures remain until the vehicle reaches the lower inflection point of the pitching motion cycle at 0°.

Examining the transient vehicle total pressure scenes, figure 4.11, shows the unsteady flow leads to lower pressure in the underbody and engine compartment region for the upstoke than in the downstroke, thus leading to the aerodynamic coefficient hysteresis seen in Figure 4.6.

4.4 Reduced Order Aerodynamic Model

Comparing the aerodynamic coefficients resulting from the ±0.5°, 4 Hz pitching motion test to the static vehicle tests reveals the transient effects are most prominent on the drag, lift, and pitch moment coefficients; thus, these aerodynamic coefficients are the focus for the reduced order aerodynamic model development and validation.

4.4.1 Model Structure

The quasi steady state aerodynamic models currently used in industry can be complex and functions of many independent variables[13]. The reduced order aerody-

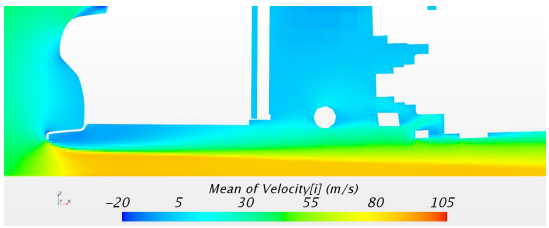

(a)

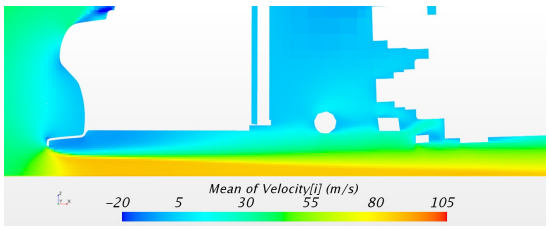

(b)

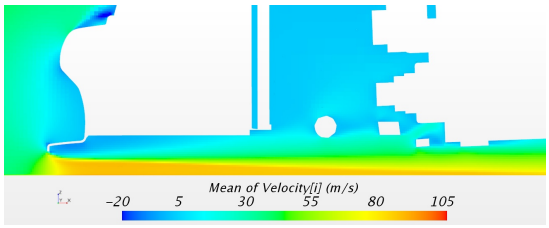

(c)

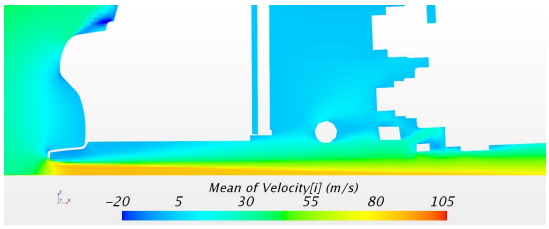

(d)

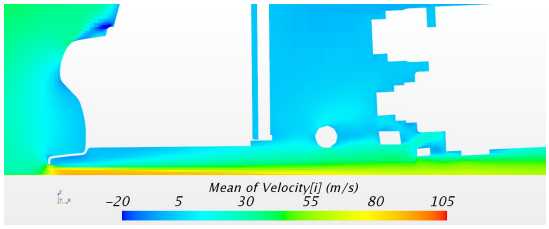

(e)

Figure 4.7: Mean X-velocity scenes from each static vehicle pitch angle simulation; (a) 1° pitch angle; (b) 0.75° pitch angle; (c) 0.5° pitch angle; (d) 0.25° pitch angle; (e) 0° pitch angle

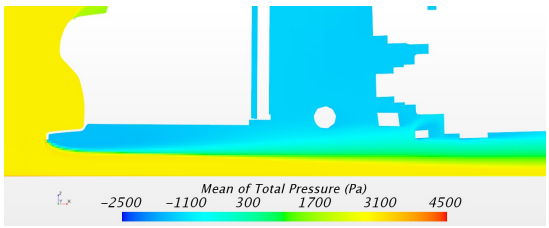

(a)

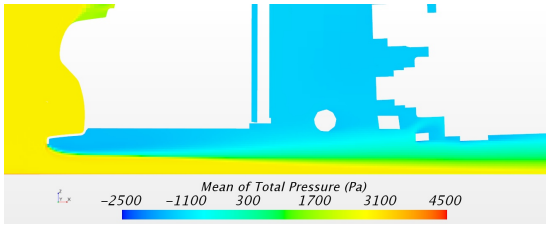

(b)

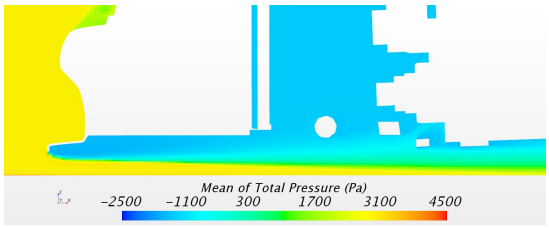

(c)

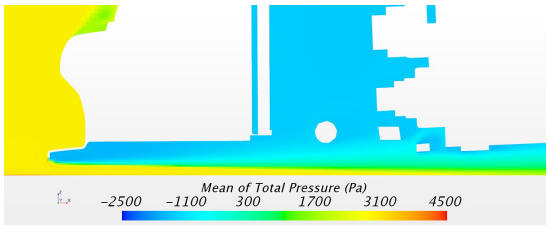

(d)

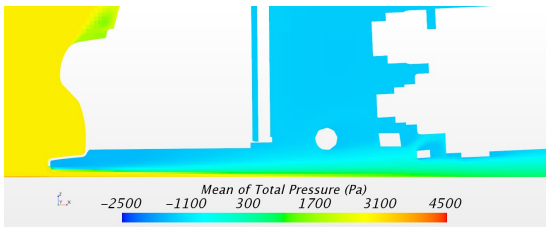

(e)

Figure 4.8: Mean total pressure scenes from each static vehicle pitch angle simulation; (a) 1° pitch angle; (b) 0.75° pitch angle; (c) 0.5° pitch angle; (d) 0.25° pitch angle; (e) 0° pitch angle

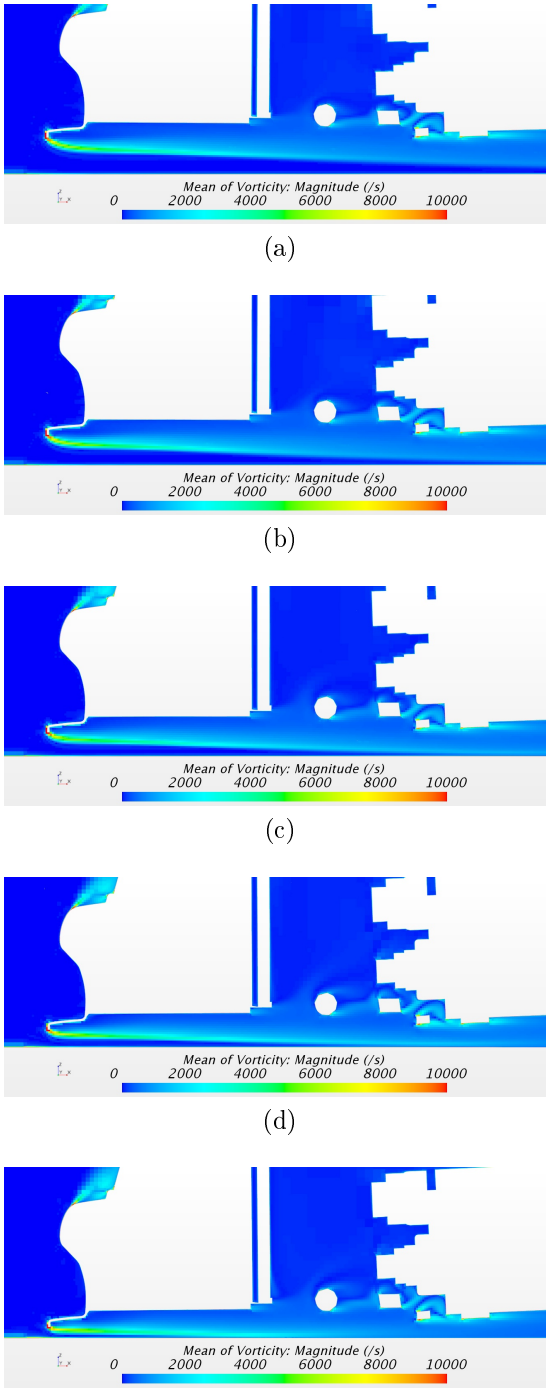

(a)

(b)

(c)

(d)

(e)

Figure 4.9: Mean vorticity magnitude scenes from each static vehicle pitch angle simulation; (a) 1° pitch angle; (b) 0.75° pitch angle; (c) 0.5° pitch angle; (d) 0.25° pitch angle; (e) 0° pitch angle

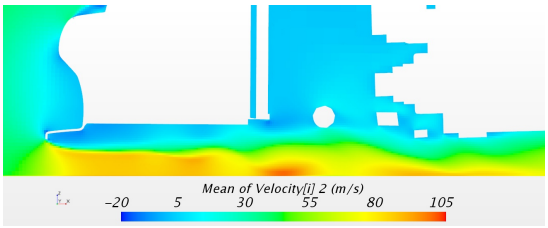

(a)

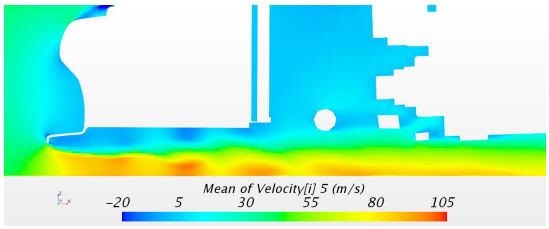

(b)

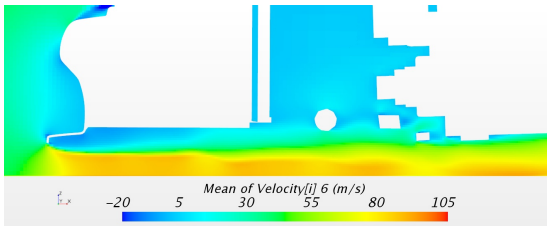

(c)

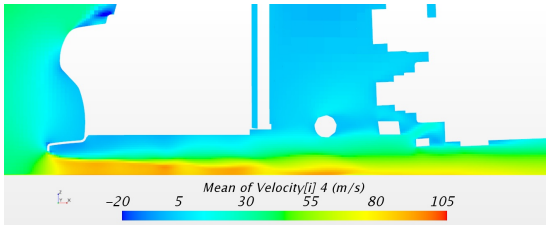

(d)

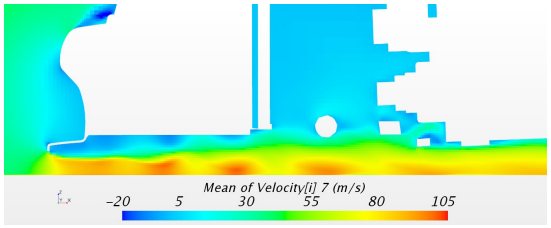

(e)

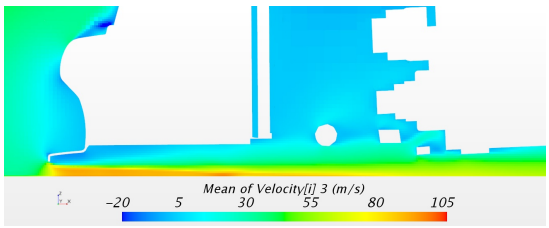

(f)

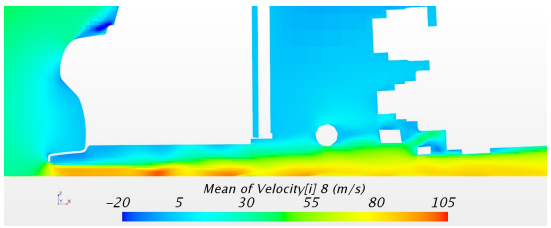

(g)

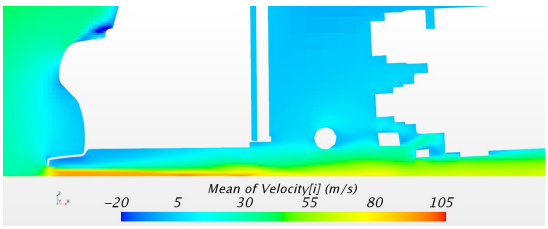

(h)

Figure 4.10: Phase averaged X-velocity scenes throughout a pitch cycle; (a) 1° pitch angle; (b) 0.75° pitch angle, upstroke; (c) 0.75° pitch angle, downstroke; (d) 0.5° pitch angle, upstroke; (e) 0.5° pitch angle, downstroke; (f) 0.25° pitch angle, upstroke; (g) 0.25° pitch angle, downstroke; (h) 0° pitch angle

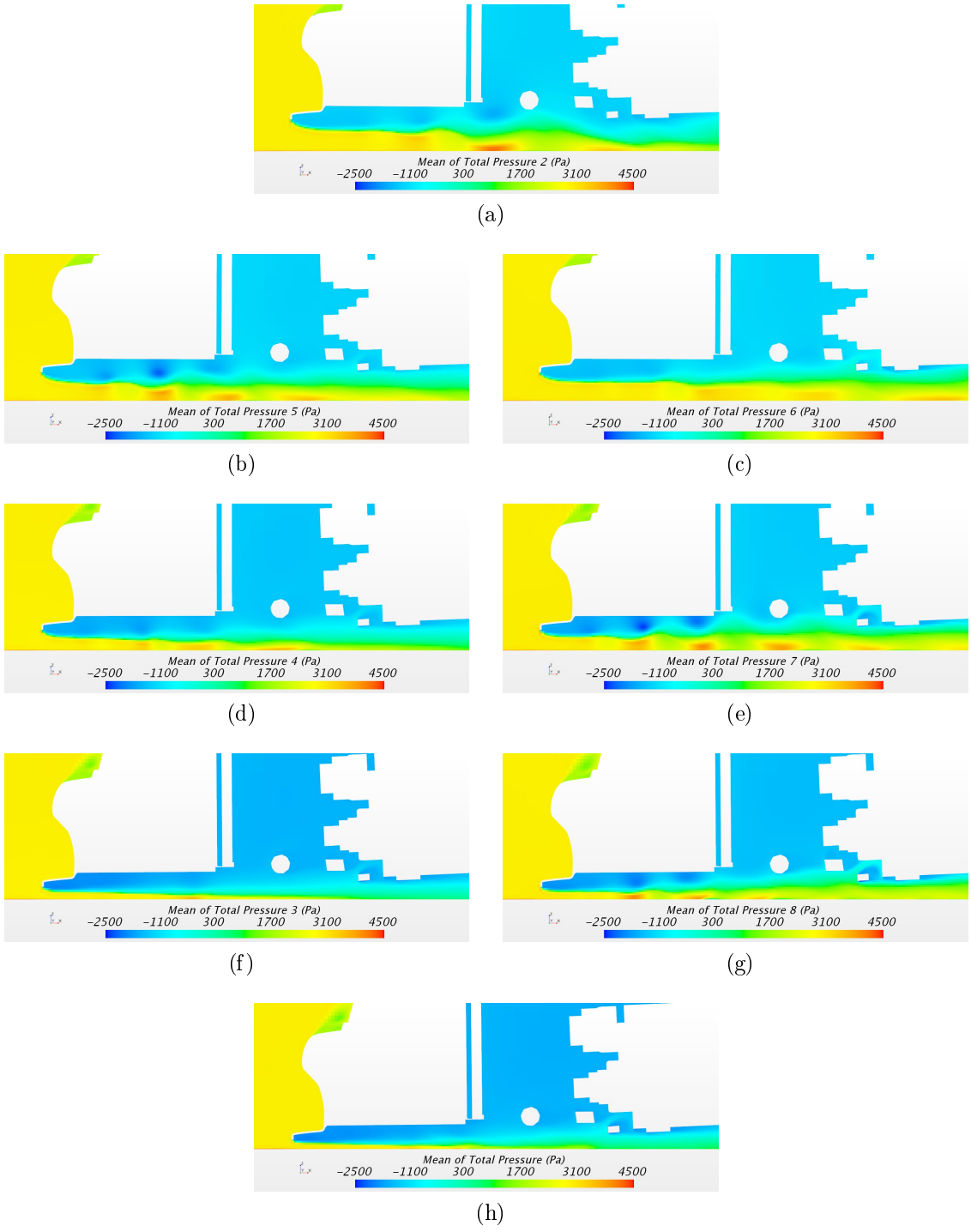

Figure 4.11: Phase averaged total pressure scenes throughout a pitch cycle; (a) 1° pitch angle; (b) 0.75° pitch angle, upstroke; (c) 0.75° pitch angle, downstroke; (d) 0.5° pitch angle, upstroke; (e) 0.5° pitch angle, downstroke; (f) 0.25° pitch angle, upstroke; (g) 0.25° pitch angle, downstroke; (h) 0° pitch angle

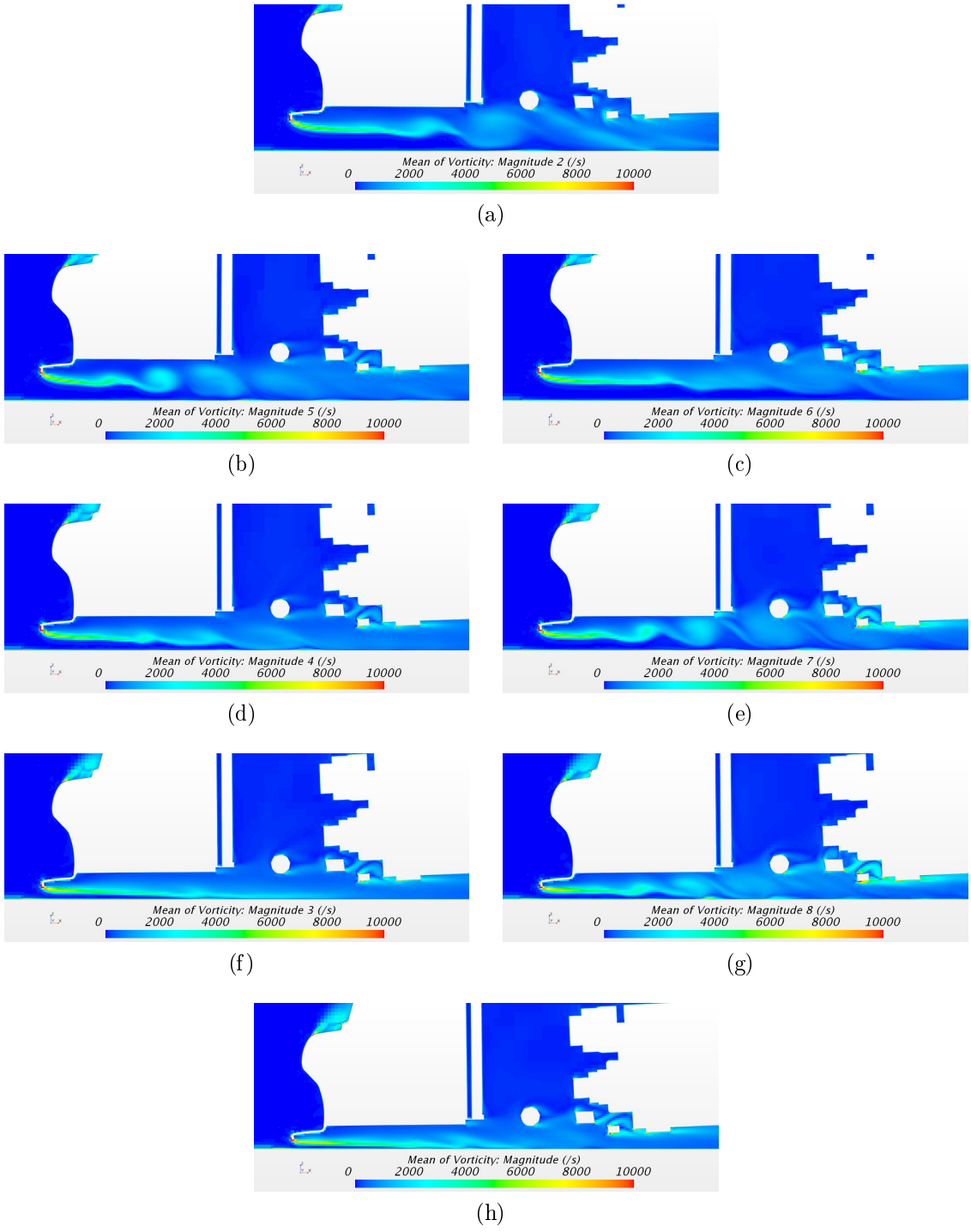

Figure 4.12: Phase averaged vorticity magnitude scenes throughout a pitch cycle; (a) 1° pitch angle; (b) 0.75° pitch angle, upstroke; (c) 0.75° pitch angle, downstroke; (d) 0.5° pitch angle, upstroke; (e) 0.5° pitch angle, downstroke; (f) 0.25° pitch angle, upstroke; (g) 0.25° pitch angle, downstroke; (h) 0° pitch angle

namic model developed in this research is a function of a single independent variable, pitch angle, as this is the only independent variable varied in this study. As future research is conducted, the reduced order aerodynamic model can be expanded to include the effects of other independent variables.

To capture the differences between the quasi steady state and transient aerodynamic coefficients, the reduced order aerodynamic model modularly combines the quasi steady state model and the transient ROM with the structure diagrammed in figure 4.13 where α is the pitch angle of the vehicle, $C_{pred,x}$ is the predicted aerodynamic coefficient x, and $C_{QSS,x}$ and $C_{T,x}$ are the quasi steady state and transient components, respectively, of the predicted aerodynamic coefficient. The modularity of this model structure allows for the implementation of the transient aerodynamic ROM with any quasi steady state model currently used in industry.

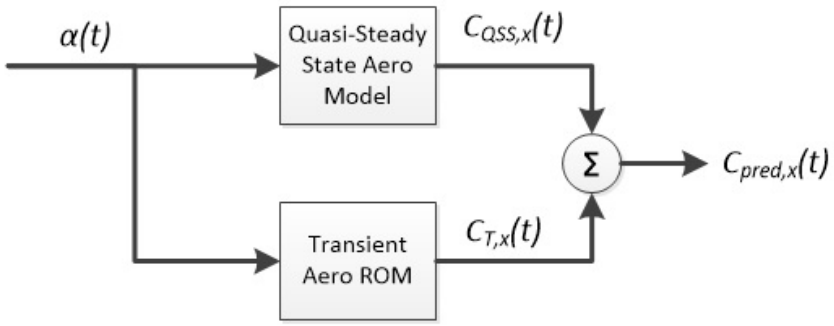

Figure 4.13: Reduced order aerodynamic model structure

For this study, a simplified quadratic quasi steady state model is developed for each of the aerodynamic coefficients based on the static vehicle simulation results such that

$$C_{QSS,x} = K_{2,x}\alpha^2 + K_{1,x}\alpha + K_{0,x} \tag{4.1}$$

where $K_{2,x}$, $K_{1,x}$, and $K_{0,x}$ are derived from applying a quadratic fit to the aerodynamic coefficient from the static vehicle with respect to the pitch angle.

The transient component of the each aerodynamic coefficient, $C_{T,x}$, is thus

$$C_{T,x} = C_x - C_{QSS,x} \tag{4.2}$$

The structure of the transient ROM is determined by analyzing the results from a transient CFD simulation with a 0.5° mean, 25 Hz band-limited white nose pitching motion applied to the vehicle. The frequency response of $C_{T,x}$ is first calculated with respect to $\Delta\alpha$, the pitch angle deviation from α_0, the mean pitch angle of the band-limited white noise motion. A transfer function representing the transient ROM is then fit to each frequency response function using Levy's theory of complex curve fitting [12] thus linearizing the transient ROM about α_0. The defines the proposed transient aerodynamic ROM structure shown in figure 4.14.

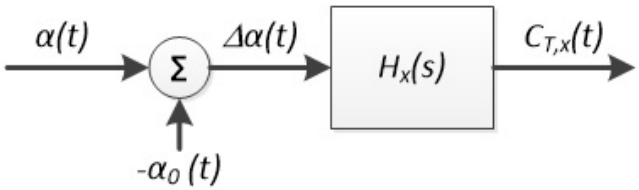

Figure 4.14: Transient aerodynamic ROM structure

The frequency responses are generated using a 1 s long Hamming window with 50% overlap providing a frequency resolution of 1 Hz. The four seconds of simulation time and the 50% overlap allow for seven windows to be averaged to reduce computational noise. The simulation time step of 2e-4 produces a frequency response up to 2500 Hz; however, this analysis focuses on the content below 25 Hz as the system input is band-limited at 25 Hz. The frequency response functions are shown in figures 4.15 - 4.17.

At lower frequencies, the frequency responses do not represent a linear system well. To better understand the root cause of this, Fourier transforms of the aerodynamic coefficients from the static vehicle and 4 Hz pitching motion CFD simulations, shown

in figure 4.18, are analyzed. The Fourier transforms for the pitching vehicle aerodynamic coefficients contain an expected peak at 4 Hz due to the system response to the applied 4 Hz pitching motion. Interestingly, there is additional frequency content shown in the Fourier transforms which occurs in both the static and pitching vehicle simulations around 1-2 Hz and in the 6-7 Hz range. This is attributed to the unsteady flow around the vehicle caused by the vortex shedding [16, 7]. The identification of the two modes of vortex shedding is also consistent with the previous findings of Grandemange et al.[7] who identified a similar occurrence when experimentally studying the flow past a blunt body positioned close to the ground plane.

The amplitude of the frequency content at 1 Hz is 0.013 for the drag coefficient, 0.035 for the lift coefficient, and about 0.02 for the pitch moment coefficient. When comparing this frequency content to the Fourier transform of the aerodynamic coefficients from the band-limited white noise simulation, figure 4.19, they are shown to be similar in magnitude. This reveals that in the band-limited white noise simulation there is minimal content in this frequency range resulting from the linear system response to the input signal, and the frequency content in this range is primarily a function of the unsteady flow dynamics.

When attempting to identify the linear system, this unsteady flow content is essentially noise on the output signal, and the amplitude of this noise dominates any content resulting from the linear system. Utilizing the data for these lower frequencies is invalid for fitting the transfer functions. The transfer functions will thus be fit using the frequency content above 7 Hz. While this is a limitation to the development of the transient model, the assumption is made that characterizing the dynamics from 7-25 Hz will yield a sufficient transient model, and this assumption will be verified by validating the model against an additional CFD simulation. Future research should be conducted to better understand the lower frequency vortex shedding and determine how to account for these effects in the transient model.

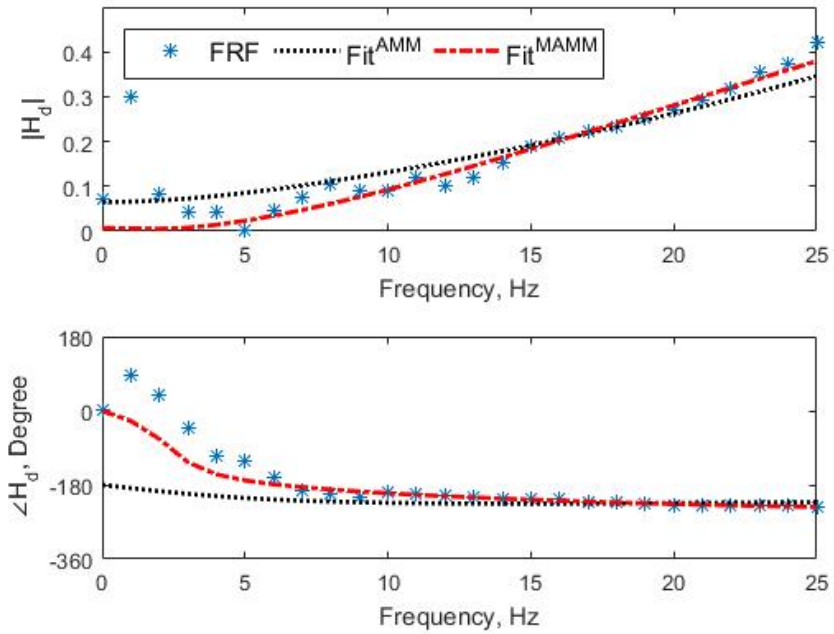

Figure 4.15: Frequency response function and transfer function fits used to generate the transient aerodynamic model coefficients for C_d

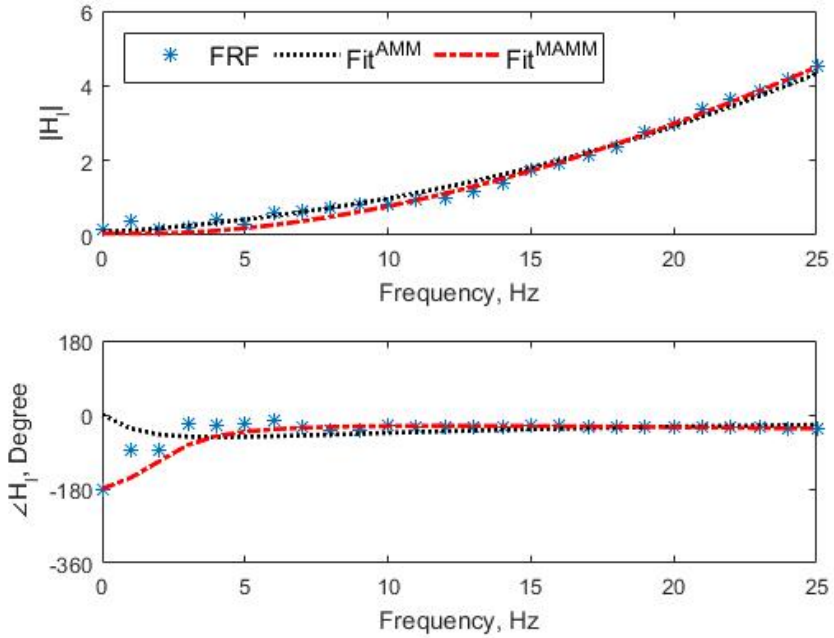

Figure 4.16: Frequency response function and transfer function fits used to generate the transient aerodynamic model coefficients for C_l

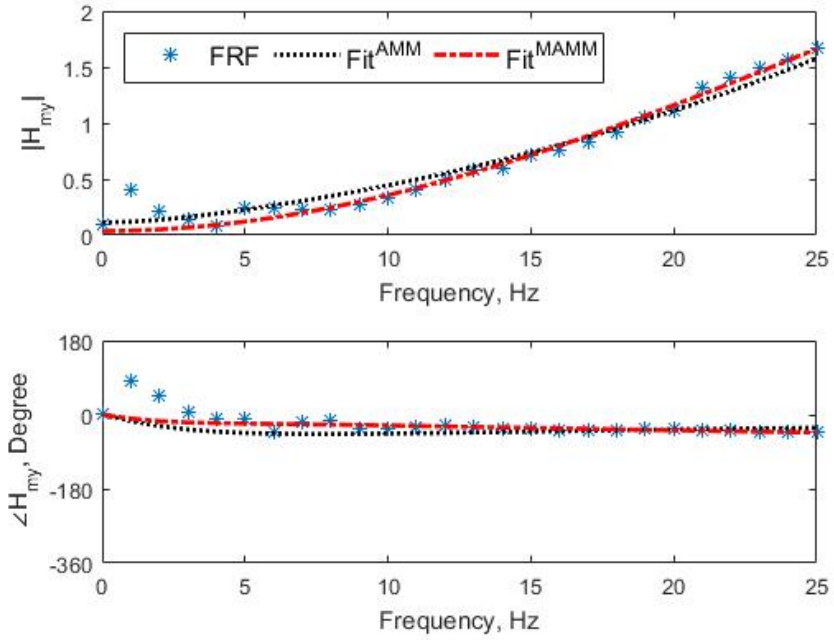

Figure 4.17: Frequency response function and transfer function fits used to generate the transient aerodynamic model coefficients for C_{my}

The initial proposed structure for the transient aerodynamic ROMs, $H_x(s)$, follows the added mass theory, [9], which is defined as

$$C_{T,x}(t) = C_{3,x}\ddot{\alpha}(t) + C_{2,x}\dot{\alpha}(t) + C_{1,x}\alpha(t) \tag{4.3}$$

where $C_{3,x}$, $C_{2,x}$, and $C_{1,x}$ are experimentally determined coefficients.

This structure is the same as the aerodynamic model structures proposed by Nakashima et al. [15] and Tsubokura et al. [17]. Taking the Laplace transform of equation 4.3 and setting the initial conditions to zero yields the second order transfer function, referred to as the added mass model (AMM),

$$\frac{C_{T,x}(s)}{\Delta\alpha(s)} = C_{3,x}s^2 + C_{2,x}s + C_{1,x} \tag{4.4}$$

$C_{3,x}$, $C_{2,x}$, and $C_{1,x}$ can be found by fitting equation 4.4 to the frequency responses.

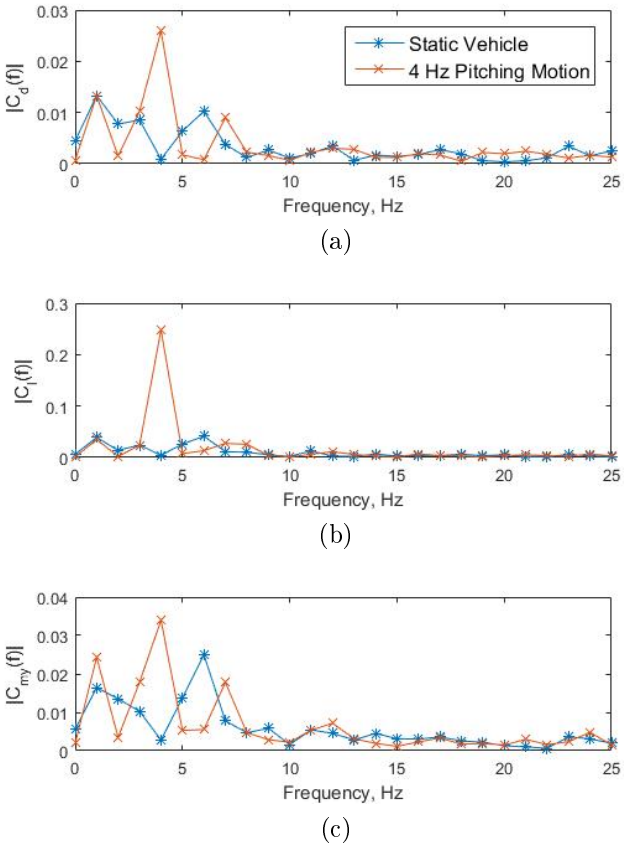

Figure 4.18: Fourier transforms of the aerodynamic coefficients from the static vehicle and 4 Hz pitching motion CFD simulations; (a) Drag coefficient, C_d; (b) Lift coefficient, C_l; (c) Pitch moment coefficient, C_{my}

The frequency responses and AMM transfer function fits are shown in figures 4.15 - 4.17. In the 7-25 Hz frequency range, the fit of the AMM transfer function, shown in figure 4.16, captures the lift frequency response well. However, the AMM transfer function fit does not fit the drag and pitch moment frequency response as well as shown in figure 4.15 and 4.17, respectively. The fit over predicts the magnitude of the responses at lower frequencies in the 7-10 Hz range while under predicting the magnitude at higher frequencies in the 20-25 Hz range. Based on the shape of the drag and pitch moment frequency responses, an additional term is added to the proposed transient ROM such that the revised transfer function, referred to as the modified

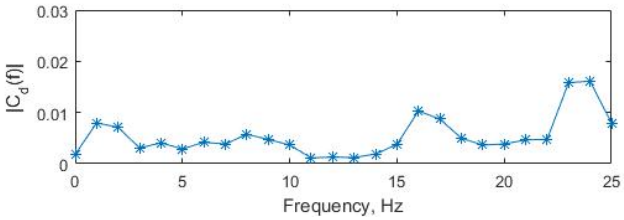

(a)

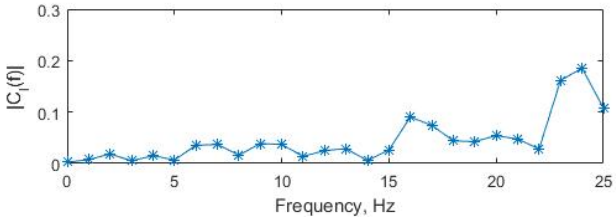

(b)

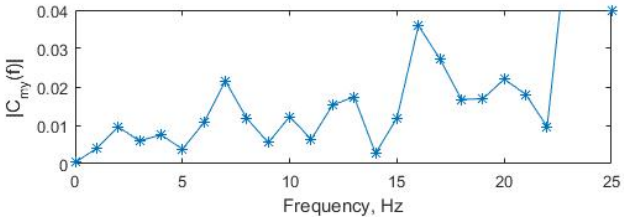

(c)

Figure 4.19: Fourier transforms of the aerodynamic coefficients from the band-limited white noise simulation; (a) Drag coefficient, C_d; (b) Lift coefficient, C_l; (c) Pitch moment coefficient, C_{my}

added mass model (MAMM), takes the form

$$\frac{C_{T,x}(s)}{\Delta\alpha(s)} = \frac{C_{3,x}s^2 + C_{2,x}s + C_{1,x}}{s + C_{4,x}} \tag{4.5}$$

Fitting this MAMM transfer function to the frequency responses, shown in figures 4.15 - 4.17, yields improved transfer function fits.

Overall, the MAMM provides representative fits of the frequency response functions in the 7-25 Hz frequency range and as such is the proposed transient aerodynamic ROM.

4.4.2 Model Validation

An additional transient vehicle CFD simulation is conducted to validate the reduced order aerodynamic model proposed in this study. This simulation applies a 0.5° mean, 25 Hz band-limited white noise pitching motion to the vehicle body which is uncorrelated with the motion used to characterize the model. The pitch angle of the vehicle body recorded from the CFD simulation is input into the reduced order aerodynamic model including the MAMM transient ROM to predict the drag, lift, and pitch moment coefficients. These predicted coefficients are compared to the CFD results in figures 4.20 - 4.22. The predicted drag, lift, and pitch moment coefficients are also calculated using the reduced order aerodynamic model developed with the AMM transient ROM and overlayed with the results in figures 4.20 - 4.22 to quantify the improved accuracy of the MAMM. The results from the quasi steady state aerodynamic model are also included in figures 4.20 - 4.22 to provide an understanding of the aerodynamic coefficient correction provided by the transient aerodynamic ROM. Each validation figure contains a plot of the aerodynamic coefficient comparison spanning a full second to provide a broader view of the correlation and a plot zoomed in to span 0.15 seconds to provide a more detailed comparison between the aerodynamic coefficients.

The reduced order aerodynamic model with the MAMM transient ROM is shown to predict the drag, lift, and pitch moment aerodynamic coefficients well and improves the prediction of the coefficients over the reduced order aerodynamic model with the AMM transient ROM. The sum squared error is calculated between each of the models and the CFD results, and the MAMM is shown to reduced the sum squared error by 43%, 51%, and 50% for the drag, lift, and pitch moment coefficients, respectively. Even thought the transient models are developed without fitting to the frequency response content below 7 Hz, the models are still shown to correlate well to the CFD results.

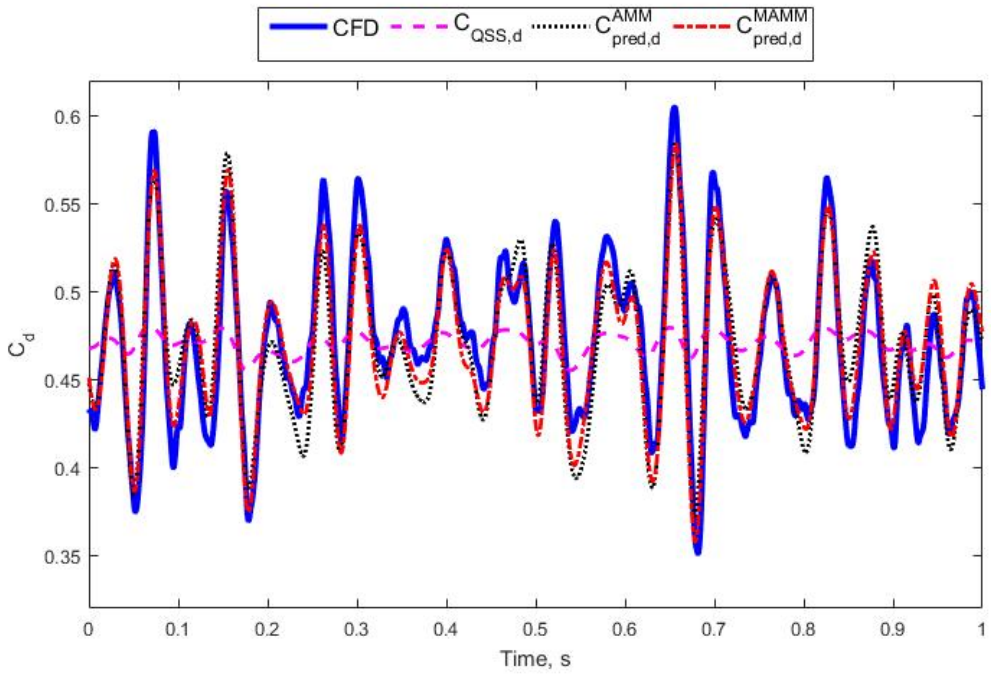

(a)

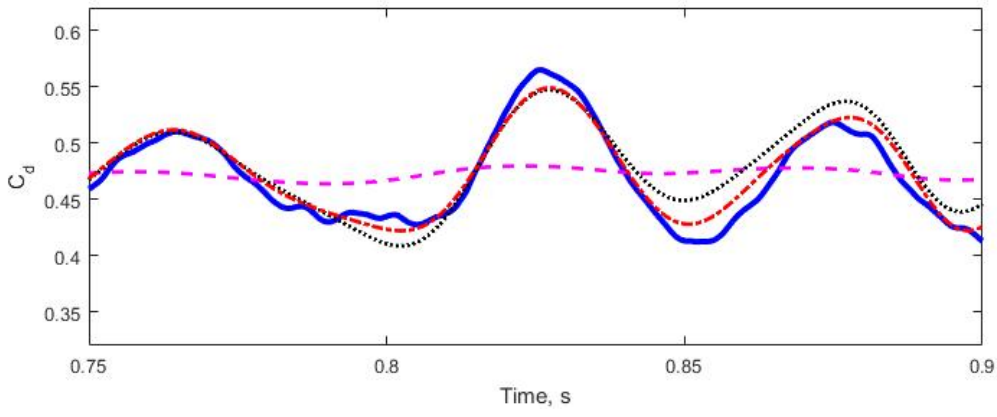

(b)

Figure 4.20: Validation of the C_d transient aerodynamic model; (a) Comparison across 1 second; (b) Comparision zoomed in across 0.15 seconds

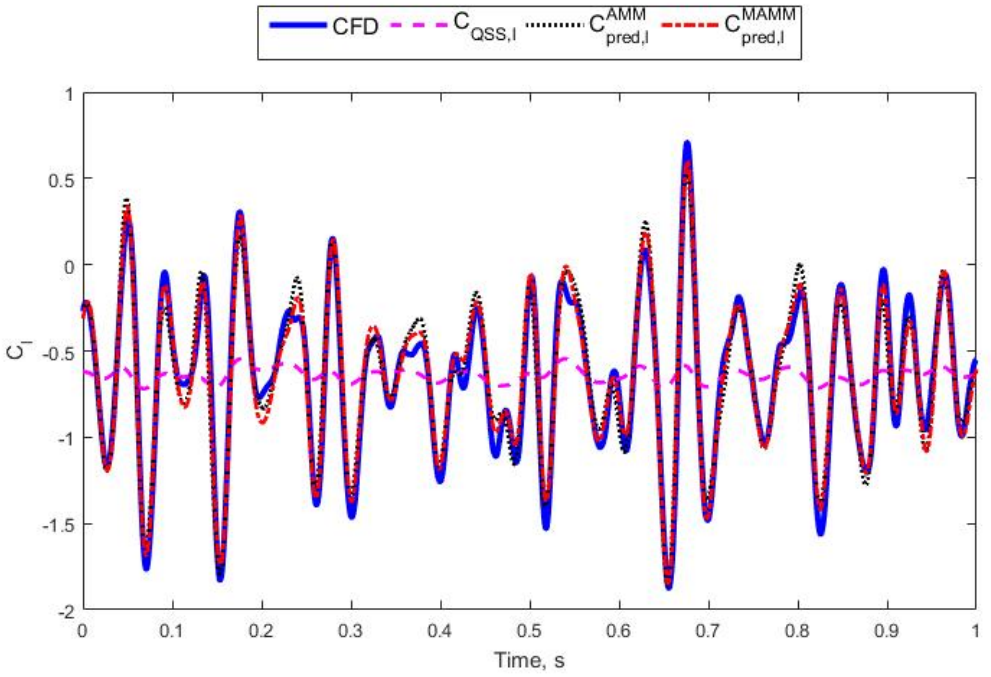

(a)

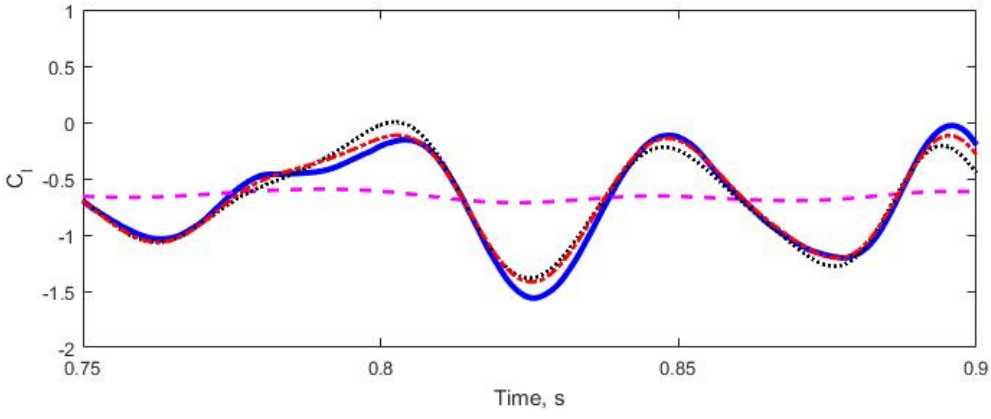

(b)

Figure 4.21: Validation of the C_l transient aerodynamic model; (a) Comparison across 1 second; (b) Comparision zoomed in across 0.15 seconds

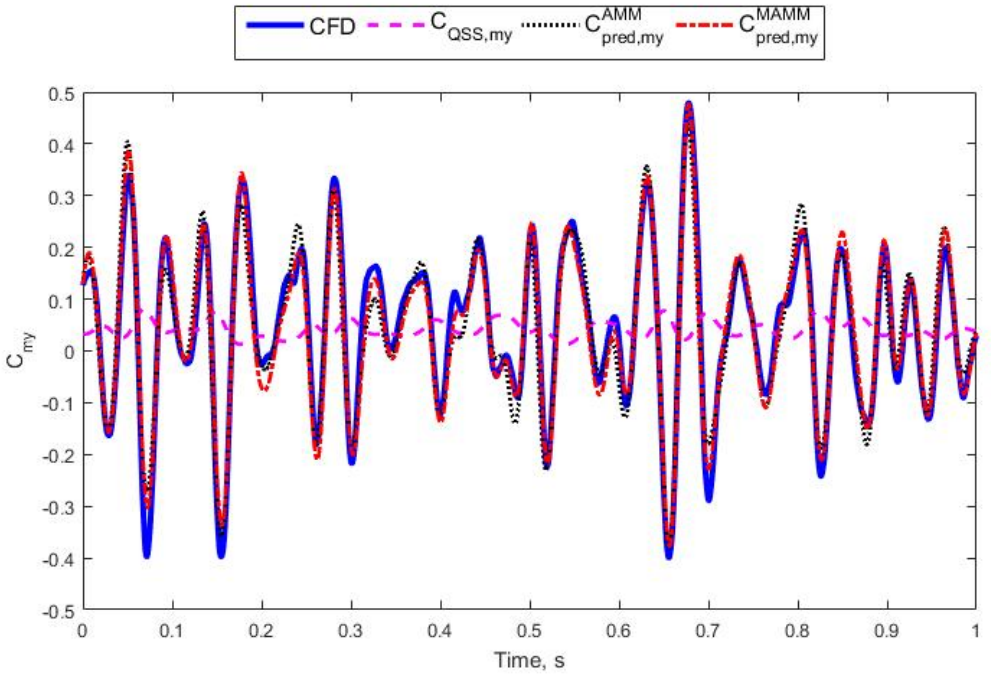

(a)

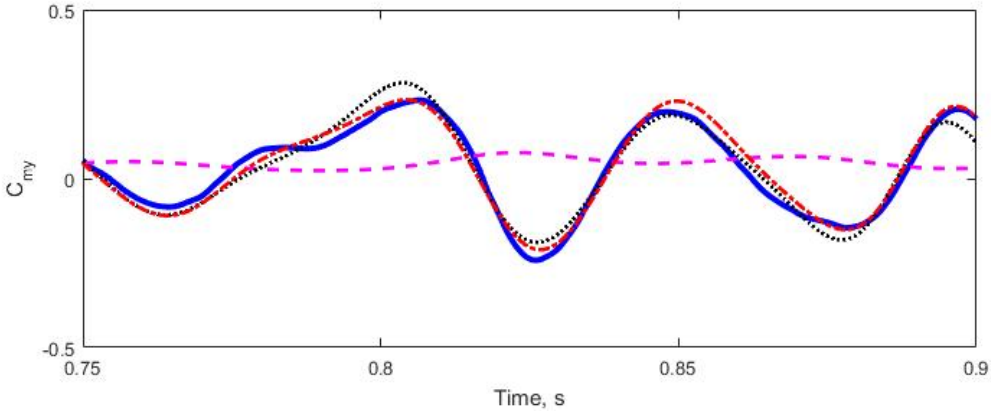

(b)

Figure 4.22: Validation of the C_{my} transient aerodynamic model; (a) Comparison across 1 second; (b) Comparision zoomed in across 0.15 seconds

The addition of the transient model to the overall aerodynamic model is a significant improvement in the model's predictive capability compared to the quasi steady state model alone. The quasi steady state model, which is currently the industry standard for aerodynamic models in vehicle dynamics simulation [13], is unable to capture the majority of the transient aerodynamic effects.

4.5 Conclusion

The $\pm 0.5°$, 4 Hz pitching motion CFD simulation reveals significant differences between the static vehicle and transient vehicle results for the drag, lift, and pitch moment coefficients whereas minimal variations are seen in the side force, roll moment, and yaw moment coefficients. This focuses the reduced order aerodynamic model development on the drag, lift, and pitch moment aerodynamic coefficients. Analyzing the flow fields shows the differences between the static and transient vehicle results originate from flow differences along the underbody in the front of the vehicle.

A new reduced-order aerodynamic model structure is proposed to couple the transient aerodynamic ROM with a quasi steady state aerodynamic model while maintaining modularity of each model within the structure. The reduced order models for the drag, lift, and pitch moment coefficients are validated against CFD data and are shown to predict the aerodynamic coefficients well with a significant predictive improvement over the quasi steady state model.

This research begins to investigate and develop reduced order models to characterize the transient aerodynamics of a race vehicle. There are many future research projects recommended to expand upon this work. Additional research can be conducted to characterize the transient effects of other independent variables, such as heave, sway, and yaw, better understand and account for the effects of the low frequency vortex shedding on the transient model, and evaluate the effect of the reduced order aerodynamic models in vehicle dynamic simulations.

REFERENCES

[1] Peter Aschwanden, Jürg Müller, and Ulrich Knörnschild. Experimental study on the influence of model motion on the aerodynamic performance of a race car. Technical Report 2006-01-0803, SAE Technical Paper, 2006.

[2] Peter Aschwanden, Jürg Müller, Gian Claudio Travaglio, and Timo Schöning. The influence of motion aerodynamics on the simulation of vehicle dynamics. *SAE International Journal of Passenger Cars-Mechanical Systems*, 1(2008-01-0657):545–551, 2008.

[3] SY Cheng, M Tsubokura, T Nakashima, Y Okada, and T Nouzawa. Numerical quantification of aerodynamic damping on pitching of vehicle-inspired bluff body. *Journal of Fluids and Structures*, 30:188–204, 2012.

[4] SY Cheng, Makoto Tsubokura, Takuji Nakashima, Takahide Nouzawa, and Yoshihiro Okada. A numerical analysis of transient flow past road vehicles subjected to pitching oscillation. *Journal of Wind Engineering and Industrial Aerodynamics*, 99(5):511–522, 2011.

[5] Jeffery P. Chrstos. *Use of vehicle dynamics modeling to quantify race car handling behavior*. dissertation, Ohio State University, Columbus, Ohio, 2001.

[6] Chen Fu, Mesbah Uddin, Clay Robinson, Arturo Guzman, and David Bailey. Turbulence models and model closure coefficients sensitivity of nascar racecar rans cfd aerodynamic predictions. *SAE International Journal of Passenger Cars-Mechanical Systems*, 10(2017-01-1547):330–344, 2017.

[7] Mathieu Grandemange, Marc Gohlke, and Olivier Cadot. Turbulent wake past a three-dimensional blunt body. part 1. global modes and bi-stability. *Journal of Fluid Mechanics*, 722:51–84, 2013.

[8] ZQ Gu, TM Huang, Z Chen, YQ Zong, and W Zeng. Large eddy simulation of the flow-field around road vehicle subjected to pitching motion. *Journal of Applied Fluid Mechanics*, 9(6), 2016.

[9] Dewey H Hodges and G Alvin Pierce. *Introduction to structural dynamics and aeroelasticity*, volume 15. Cambridge University Press, 2011.

[10] Mitsuyoshi Kawakami, Norikazu Sato, Peter Aschwanden, Juerg Mueller, Yoshihiro Kato, Masaki Nakagawa, and Eiichi Ono. Validation and modeling of transient aerodynamic loads acting on a simplified passenger car model in sinusoidal motion. *SAE International Journal of Passenger Cars-Mechanical Systems*, 5(2012-01-0447):324–339, 2012.

[11] Tetsuhiro Kawamura and Atsushi Ogawa. Effect of unsteady lift force on vehicle dynamics in heave and pitch motion. Technical Report 2014-01-0576, SAE Technical Paper, 2014.

[12] EC Levy. Complex-curve fitting. *IRE transactions on automatic control*, (1):37–43, 1959.

[13] JA Mohrfeld-Halterman and M Uddin. Quasi steady-state aerodynamic model development for race vehicle simulations. *Vehicle System Dynamics*, 54(1):124–136, 2016.

[14] Yusuke Nakae, Jun Yamamura, Hiroshi Tanaka, and Tsuyoshi Yasuki. Study of unsteady aerodynamics of a car model in dynamic pitching motion. Technical Report 2016-01-1609, SAE Technical Paper, 2016.

[15] Takuji Nakashima, Makoto Tsubokura, Takahide Nouzawa, Takaki Nakamura, and Masashi Ichimiya. Flow structures above the trunk deck of sedan-type vehicles and their influence on high-speed vehicle stability 2nd report: Numerical investigation on simplified vehicle models using large-eddy simulation. *SAE International Journal of Passenger Cars-Mechanical Systems*, 2(2009-01-0006):157–167, 2009.

[16] Brett Peters and Mesbah Uddin. Impact of longitudinal acceleration and deceleration on bluff body wakes. *Fluids*, 4(3):158, 2019.

[17] Makoto Tsubokura, See Yuan Cheng, Takuji Nakashima, Yoshihiro Okada, and Takahide Nouzawa. Simulation and analysis of effects of dynamic pitching for idealized sedan-type vehicle models. Technical Report 2011-01-0153, SAE Technical Paper, 2011.

CHAPTER 5: CONCLUSIONS

Throughout the course of this research, a procedure to create an accurate vehicle aerodynamic model is developed. The aerodynamic model follows the structure in figure 1.1 which allows for separate development of the quasi steady state and transient aerodynamic models.

A new dual range quasi steady state aerodynamic model is proposed that better predicts the aerodynamic coefficients than conventional quasi steady state aerodynamic models. A model reduction procedure is also developed for this model to reduce the terms in the model and the amount of data required to generate an accurate model.

Transient vehicle CFD simulations revealed a significant difference between the quasi steady state and transient aerodynamic coefficients mainly for the drag, lift, and pitch moment coefficients of the vehicle. Research conducted on a simpler airfoil model revealed that linear system identification techniques could be applied to properly designed CFD simulations to extract the structure of the transient ROMs required to capture the transient aerodynamic characteristics.

When applying these system identification techniques to characterize the aerodynamic effects of the vehicle in pitching motion, a new structure for the transient aerodynamic ROM was revealed. The new transient structure resulted in more accurate transient predictions than the conventional transient models currently found in literature. The transient ROM validation also revealed the importance of including the transient model in the overall aerodynamic model as the quasi steady state model alone was unable to accurately predict the transient aerodynamic coefficients.

While this work develops a complete quasi steady state aerodynamic model, the research is the beginning of the development of the complete transient aerodynamic

ROM. Future work is planned to model the transient aerodynamic effects of the vehicle in heave and yaw motion as well. Additional studies are also planned to characterize the effects of the transient aerodynamic model on the predictive capabilities of the vehicle dynamic simulation.

REFERENCES

[1] Jeffery P. Chrstos. *Use of vehicle dynamics modeling to quantify race car handling behavior*. Dissertation, Ohio State University, Columbus, Ohio, 2001.

[2] JA Mohrfeld-Halterman and M Uddin. High fidelity quasi steady-state aerodynamic model effects on race vehicle performance predictions using multi-body simulation. *Vehicle System Dynamics*, 54(7):963–981, 2016.

[3] JA Mohrfeld-Halterman and M Uddin. Quasi steady-state aerodynamic model development for race vehicle simulations. *Vehicle System Dynamics*, 54(1):124–136, 2016.